

# Switching, Multiple Time-Scales and Geometric Blow-Up in a Low-Dimensional Gene Regulatory Network

S. Jelbart, K. U. Kristiansen & P. Szmolyan

April 30, 2025

## Abstract

ODE-based models for gene regulatory networks (GRNs) can often be formulated as smooth singular perturbation problems with multiple small parameters, some of which are related to time-scale separation, whereas others are related to ‘switching’, (proximity to a non-smooth singular limit). This motivates the study of reduced models obtained after (i) quasi-steady state reduction (QSSR), which utilises the time-scale separation, and (ii) piecewise-smooth approximations, which reduce the nonlinearity of the model by viewing highly nonlinear sigmoidal terms as singular perturbations of step functions. We investigate the *interplay* between the reduction methods (i)-(ii), in the context of a 4-dimensional GRN which has been used as a low-dimensional representative of an important class of (generally high-dimensional) GRN models in the literature. We begin by identifying a region in the small parameter plane for which this problem can be formulated as a smooth singularly perturbed system on a blown-up space, uniformly in the switching parameter. This allows us to apply Fenichel’s coordinate-free theorems and obtain a rigorous reduction to a 2-dimensional system, that is a perturbation of the QSSR. Finally, we show that the reduced system features a Hopf bifurcation which does not appear in the QSSR system, due to the influence of higher order terms. Taken together, our findings suggest that the relative size of the small parameters is important for the validity of QSS reductions and the determination of qualitative dynamics in GRN models more generally. Although the focus is on the 4-dimensional GRN, our approach is applicable to higher dimensions.

**Keywords:** gene regulatory networks, model reduction, geometric singular perturbation theory, geometric blow-up, switching

**MSC2020:** 34E13, 34E15, 34E10, 94C11, 37N25

## 1 Introduction

Mathematical models of biological and biochemical phenomena often feature *switching*, i.e., abrupt dynamical transitions which occur when a particular variable or set of variables in the model cross over a threshold. In the context of ODE-based models, switching can often be described by smooth singular perturbation problems which limit to *piecewise-smooth (PWS)* systems as one or more of the perturbation parameters tend to zero. Problems of this kind have received a lot of attention in recent years; here we refer to [24, 27, 33, 44, 48, 49] for recent work on low-dimensional problems featuring switching in low-dimensional ODE models of intracellular calcium oscillation, substrate-depletion oscillation, mitotic oscillation in a model for the embryonic cell cycle, a cAMP signalling model for cell aggregation and the Jansen-Rit model in mathematical neuroscience.

In addition to switching, many biological and biochemical processes – and consequently also the mathematical models thereof – evolve on multiple time-scales. This is also true of the particular applications mentioned above, and one of the main contributions of the references [24, 27, 33, 44, 48] has been to demonstrate that switching and multiple time-scale aspects of the models can be analysed with a common set of mathematical techniques based on *geometric singular perturbation theory (GSPT)* [11, 25, 37, 52, 54] and a method of desingularisation known as *geometric blow-up* [8, 30, 35, 36, 50]. Singular perturbation analyses of problems involving both switching and multiple time-scales tend to be complicated by the presence of multiple small parameters, some of which relate to switching, whereas others are related to the multi-scale structure of the model. One approach to the analysis of these

problems is to group the small parameters together by relating them to a single small parameter, as in e.g. [24, 34, 48]. This serves to simplify the analysis, however, approaches of this kind tend to rely on the availability of good numerical estimates for the parameter values, and one cannot in general expect the same dynamics if the singular limit is approached along a different curve in parameter space. Detailed mathematical analyses of problems with multiple small parameters that describe the asymptotic behaviour and singular limit in the corresponding small parameter space, where the small parameters are kept independent, are much more involved. Perhaps unsurprisingly, analyses of this kind appear to be less common in the literature, however we refer to [1, 5, 29, 38] for notable exceptions.

## 1.1 Multiple time-scales and switching in GRNs

This article is motivated by the interplay between multiple time-scale dynamics and switching in an important class of *gene regulatory network (GRN)* models which can be traced back to the pioneering work in [17, 51]. A significant body of research investigating the dynamics and properties of these systems has emerged in recent decades, see e.g. [10, 41, 42, 46, 47] and the many references therein. The models in question can be written as  $2N$ -dimensional ODE systems of the form

$$\begin{aligned} r'_i &= F_i(h_{i,1}(p_1; \theta_1, n_1), h_{i,2}(p_2; \theta_2, n_2), \dots, h_{i,N}(p_N; \theta_N, n_N)) - \gamma_i r_i, \\ p'_i &= \varepsilon (\kappa_i r_i - \delta_i p_i), \end{aligned} \quad (1)$$

where  $(\cdot)' = \frac{d}{dt}$ ,  $i = 1, \dots, N$ ,  $r_i \geq 0$  denotes the concentration of transcribed mRNA associated with a particular gene  $i$ ,  $p_i \geq 0$  denotes the concentration of the corresponding translated protein,  $\gamma_i, \varepsilon, \kappa_i, \delta_i, \theta_i, n_i$  are strictly positive parameters, each  $h_{i,j}$  is a Hill function of the form  $h_{i,j} = h^+$  or  $h_{i,j} = h^-$ , where

$$h^-(p; \theta, n) = 1 - h^+(p; \theta, n) = \frac{\theta^n}{p^n + \theta^n}, \quad (2)$$

and each function  $F_i$  is a polynomial in its arguments. We refer to e.g. [10, 46] for details, and to Figure 1 for a graphical representation of the Hill functions  $h^\pm$ .

Either or both of the following assumptions are commonly made in order to simplify the full network (1):

- (i) **QSSR**:  $0 < \varepsilon \ll 1$ . This amounts to the assumption that mRNA transcription is very fast compared with the protein dynamics. Applying the QSSR, i.e. setting  $r'_i = 0$  for each  $i = 1, \dots, N$ , reduces the  $2N$ -dimensional network (1) to an  $N$ -dimensional *protein-only network*

$$\dot{p}_i = \frac{\kappa_i}{\gamma_i} F_i(h_{i,1}(p_1; \theta_1, n_1), h_{i,2}(p_2; \theta_2, n_2), \dots, h_{i,N}(p_N; \theta_N, n_N)) - \delta_i p_i, \quad i = 1, \dots, N,$$

with

$$r_i = \gamma_i^{-1} F_i(h_{i,1}(p_1; \theta_1, n_1), h_{i,2}(p_2; \theta_2, n_2), \dots, h_{i,N}(p_N; \theta_N, n_N)), \quad i = 1, \dots, N.$$

Here the overdot denotes differentiation with respect to slow time  $\tau = \varepsilon t$ .

- (ii) **Steep switching**: the Hill exponents satisfy  $n_i \gg 1$ , motivating a PWS approximation in which the Hill functions  $h^\pm$  (which are very steep when  $n_i \gg 1$ ) are replaced by piecewise-constant functions in accordance with

$$\lim_{n_i \rightarrow \infty} h^+(p_i; \theta_i, n_i) = \begin{cases} 0 & p_i < \theta_i, \\ 1 & p_i > \theta_i, \end{cases} \quad \lim_{n_i \rightarrow \infty} h^-(p_i; \theta_i, n_i) = \begin{cases} 1 & p_i < \theta_i, \\ 0 & p_i > \theta_i. \end{cases} \quad (3)$$

This (pointwise) convergence is sketched for increasing values of  $n_i$  in Figure 1.

Both (i) and (ii) simplify the analysis and/or simulation of the original network (1), although in very different ways. On the one hand, (i) takes advantage of the multi-scale (specifically slow-fast) structure of system (1) when  $0 < \varepsilon \ll 1$ , in order to reduce the the dimension from  $2N$  to  $N$ . On the other hand, (ii) reduces system (1) to a *piecewise-linear (PWL)* system. Although the resulting equations in this case are non-smooth, they are *linear* away from  $p_i = \theta_i$ .

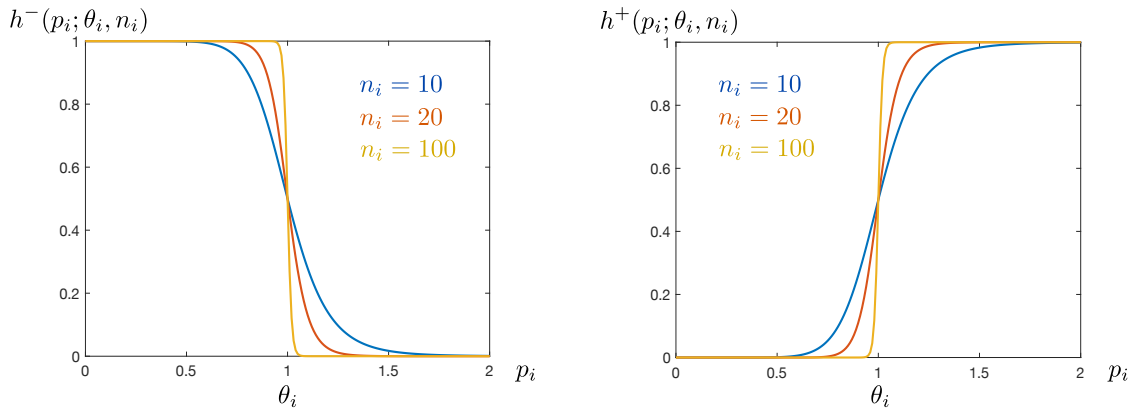


Figure 1: The Hill functions  $h^-(p_i; \theta_i, n_i)$  and  $h^+(p_i; \theta_i, n_i)$  are shown in the left and right panels respectively, for  $\theta_i = 1$  and three different values of  $n_i$ . Both functions converge to a discontinuous step function when  $n_i \rightarrow \infty$ , as in (3).

The assumption in (i) is very common in the literature, and often assumed implicitly, however we refer to [10, 16, 46] for studies which involve the mRNA variables. (It is also important to note that this assumption may not always be justified; see [15, 16] (p. 10,958 second paragraph in the former) for experimental values in actual GRN's, which demonstrate that the time-scale separation between the  $r_i$  and  $p_i$  variables varies for different applications.) The authors in [10] in particular proved a number of reduction theorems in which the QSSR can be made rigorous via a slow manifold reduction based on Fenichel theory. These results are valid for fixed  $n_i$ , as  $\varepsilon \rightarrow 0$ . In contrast, with this paper we begin a research program where we are interested in the combined limit  $n_i \rightarrow \infty$ ,  $\varepsilon \rightarrow 0$  and on the *interplay* between the reduction assumptions in (i) and (ii) above. More broadly, we are interested in whether – and if so how – the qualitative dynamics depends on the relative sizes of the small parameters associated with switching and multi-scale structure.

Numerous approaches to the non-smooth limit in (ii) appear in the literature: see [2, 18] for analyses based on Filippov theory [12], and [21, 45] for foundational work on approaches based on singular perturbation methods. Both approaches have their pros and cons. On one hand, approaches based on Filippov theory are ‘consistent’ on the PWS level, however, the dynamics prescribed at discontinuity sets may not accurately represent the dynamics of the original network (4), which is smooth. On the other hand, approaches based on singular perturbation approach can sometimes be ‘restrictive’ [10], simply due to the complicated nature of the relationship between the original network and the non-smooth limit. We refer to [41, 42, 43] for more on the relationship between these two approaches, and additional work from a singular perturbations standpoint. For the most part, the analyses presented in these works describe the limiting dynamics in reduced protein-only systems. In other words, the QSSR is applied first (or it is implicitly assumed and the analysis starts with a protein-only system), after which an asymptotic analysis as the Hill coefficients  $n_i \rightarrow \infty$  is undertaken. We also refer to [14] and the many references therein for details on an interesting approach to the study of global dynamics of switching systems based on combinatorial, topological and computational methods, which has direct significance for the study of GRNs.

## 1.2 The model

In this paper, we consider the following 4-dimensional activator-inhibitor model:

$$\begin{aligned}
 r'_a &= h^+(p_b; 1, \sigma^{-1}) - r_a, \\
 r'_b &= h^-(p_a; 1, \sigma^{-1}) - \gamma r_b, \\
 p'_a &= \varepsilon (\xi_a r_a - p_a), \\
 p'_b &= \varepsilon \delta (\xi_b r_b - p_b).
 \end{aligned} \tag{4}$$

System (4) is in the general form (1) with two Hill functions appearing on the right-hand side with  $\theta_a = \theta_b = 1$  and

$$n_a = n_b = \sigma^{-1}, \quad (5)$$

so that  $\sigma \rightarrow 0$  corresponds to the switching limit  $n_a = n_b \rightarrow \infty$ . We consider  $\varepsilon, \sigma > 0$  as independent small parameters, and  $\delta, \gamma, \xi_i, i \in \{a, b\}$  all positive and fixed in some compact set; in particular, we will treat  $\xi_a$  and  $\xi_b$  as bifurcation parameters (fixed in some compact set).

The notation and formulation in system (4) agrees with [46, eqn. (41)], except for the fact that we have assumed (5) and introduced certain scalings to eliminate extra parameters; we refer to Appendix A below for details on this derivation. The reader is also referred to [53] (where to the best of our knowledge, the system first appeared) for an earlier analysis and biochemical interpretation of system (4). We also refer to [6, 9, 19] for analyses of similar systems that involve additional terms which model self-regulation effects.

Applying a QSSR to system (4), based on  $0 < \varepsilon \ll 1$ , leads to the 2-dimensional protein-only system

$$\begin{aligned} \dot{p}_a &= \xi_a h^+(p_b; 1, \sigma^{-1}) - p_a, \\ \dot{p}_b &= \delta(\xi_b \gamma^{-1} h^-(p_a; 1, \sigma^{-1}) - p_b), \end{aligned} \quad (6)$$

with  $r_a$  and  $r_b$  slaved according to

$$r_a = h^+(p_b; 1, \sigma^{-1}), \quad r_b = \gamma^{-1} h^-(p_a; 1, \sigma^{-1}). \quad (7)$$

Since the divergence of the vector field associated with system (6) is  $-1 - \delta < 0$  for all  $\sigma > 0$ , we conclude the following:

**Lemma 1.1.** *The QSSR system (6) does not support limit cycles.*

The reduction of system (4) to the reduced protein-only system (6) can be justified using Fenichel theory [11, 25], since (7) defines a critical manifold  $\mathcal{M}(\sigma)$  of (4) for  $\varepsilon = 0$  and any  $\sigma > 0$ . It is attracting and normally hyperbolic, since the linearization of (7) gives  $-1$  and  $-\gamma^{-1}$  as the nonzero eigenvalues. Consequently, Fenichel theory provides the existence of a slow manifold for all  $0 < \varepsilon \ll 1$ , and the dynamics on the slow manifold is a smooth perturbation of the QSSR system (6). However, this result is not uniform with respect to  $\sigma \rightarrow 0$ , due to loss of smoothness along the codimension-1 *switching manifold*

$$\Sigma := \Sigma_a \cup \Sigma_b, \quad (8)$$

where

$$\Sigma_a = \{(r_a, r_b, 1, p_b) : r_a, r_b, p_b \geq 0\}, \quad \Sigma_b = \{(r_a, r_b, p_a, 1) : r_a, r_b, p_a \geq 0\}, \quad (9)$$

recall (3). This indicates that the double limit as both  $\varepsilon \rightarrow 0$  and  $\sigma \rightarrow 0$  needs a careful analysis.

### 1.3 Main results

Our main results establish the existence of a region in the  $(\sigma, \varepsilon)$  small parameter plane for which the reduction to a 2-dimensional protein-only system is possible. They also describe certain aspects of the dynamics of this reduced problem, which should be compared with the QSSR system (6).

**Theorem 1.2.** *Consider system (4) with*

$$\varepsilon = \mu\sigma, \quad (10)$$

*and fix any  $k \in \mathbb{N}$ ,  $\sigma_0 > 0$  sufficiently small and any connected compact domain  $K \subset [0, \infty)^2$ . Then the following assertions are true:*

1. *There exists a  $\mu_0 > 0$  small enough such that there exists a 2-dimensional attracting and locally invariant manifold  $\mathcal{M}_\mu(\sigma)$  for all  $\mu \in (0, \mu_0)$ ,  $\sigma \in (0, \sigma_0)$ , with  $\mu_0$  independent of  $\sigma$ , which is*

- (a) *a  $C^k$ -smooth graph over  $(p_a, p_b) \in K$ , depending smoothly upon  $\sigma \in (0, \sigma_0)$  and  $\mu \in [0, \mu_0)$ ;*

(b)  $C^0$   $\mathcal{O}(\mu)$ -close to the critical manifold  $\mathcal{M}_0(\sigma) \subset \mathcal{M}(\sigma)$  defined by the QSSR approximation in (7), uniformly with respect to  $\sigma$ .

2. Let

$$\alpha := \frac{\gamma(1 + \delta)}{\delta(1 + \gamma)}. \quad (11)$$

Then the ray defined by

$$\mu = \alpha\sigma, \quad \sigma > 0,$$

divides the  $(\sigma, \mu)$ -parameter plane into two separate regions, where Hopf bifurcations on  $\mathcal{M}_\mu(\sigma)$  (as  $(\sigma, \mu) \rightarrow (0, 0)$ ) only occur (for some values of our bifurcation parameters  $(\xi_a, \xi_b)$ ) within  $\{(\sigma, \mu) : \mu > \alpha\sigma\}$ .

3. Fix  $\mu > 0$  and consider  $\sigma \rightarrow 0$ . There exists a domain  $K'$  on which there does not exist a 2-dimensional locally invariant manifold of system (4) which is  $C^0$   $o(1)$ -close (uniformly over the domain  $K'$ ) to the QSSR manifold  $\mathcal{M}(\sigma)$  as  $\sigma \rightarrow 0$ .

Figure 2 shows a schematic representation of Theorem 1.2 in the  $(\sigma, \varepsilon)$  small parameter plane. Here, the invariant manifold  $\mathcal{M}_\mu(\sigma)$  (see assertion 1) exists in the triangular region bounded below the line  $\varepsilon = \mu_0\sigma$ . Figure 2 also showcases assertion 2; notice that the line  $\mu = \alpha\sigma$  becomes  $\varepsilon = \alpha\sigma^2$  in the  $(\sigma, \varepsilon)$ -plane. This curve distinguishes (asymptotically as  $(\sigma, \varepsilon) \rightarrow (0, 0)$ ) subregions within which it is possible or impossible for the system to undergo a Hopf bifurcation under variation of  $\xi_a$  and  $\xi_b$ ; these are the regions in shaded red and blue respectively. We will present a more detailed statement regarding the curve  $\varepsilon = \alpha\sigma^2$  below in Proposition 3.4.

The fact that the reduced system on  $\mathcal{M}_\mu(\sigma)$  – which depends upon higher order corrections that are not accounted for in a QSSR, see (6) – may or may not undergo a Hopf-type bifurcation depending on the size of  $\mu$  (cf. assertion 2 of Theorem 1.2), shows that equation (10) with  $0 < \mu \ll 1$  is necessary but not sufficient for the validity of the QSSR (loosely speaking, we consider a QSSR to be ‘valid’ if it predicts the same qualitative dynamics as the original non-reduced problem). In particular, our results show that QSSR is *not valid* in the red region of Figure 2, cf. Lemma 1.1, even though  $0 < \mu \ll 1$ .

**Remark 1.3.** The manifold  $\mathcal{M}_\mu(\sigma)$  can be treated like a ‘global’ invariant manifold in many cases, since it is forward invariant on suitably chosen but arbitrarily large choices of the compact set  $K$ . For example, if  $K = [0, A] \times [0, B]$  for any arbitrarily large but fixed  $A, B > 0$  satisfying  $A > \xi_a$  and  $B > \xi_b\gamma^{-1}$ , then  $\mu_0 > 0$  can be chosen sufficiently small that the manifold  $\mathcal{M}_\mu(\sigma)$  is forward invariant as a graph over  $K$  for all  $0 < \mu < \mu_0$ .

**Remark 1.4.** Assertion 3 of Theorem 1.2 shows that system (4) with  $\varepsilon = \mu\sigma$ ,  $\mu > 0$  fixed,  $0 < \sigma \ll 1$ , cannot in general be reduced to a protein-only system that remains  $o(1)$ -close to the QSSR over the entire physically relevant domain. However, it is still possible to perform (rigorous) local reductions as long as we stay uniformly away from  $\Sigma$ . This is also true for the general network (1) (with  $\Sigma = \cup_{i=1}^N \{p_i = \theta_i\}$ ) and it is a consequence of the fact that the limits (3) are uniform with respect to  $p_i \geq 0$  on compact intervals  $[a, b]$ ,  $0 \leq a < b$ , with  $\theta_i \notin [a, b]$ .

**Remark 1.5.** The authors in [46] showed that the Hopf-type bifurcation observed in system (4) ‘disappears’ after QSSR, when  $\sigma > 0$  is kept fixed and positive. This is consistent with Theorem 1.2, and can be understood in terms of Figure 2: taking  $\varepsilon \rightarrow 0$  along any fixed line  $\sigma > 0$  will lead to a limiting system which corresponds to a point on the positive  $\sigma$ -axis, which is contained within the shaded blue region where Hopf bifurcation is not possible. Notice, however, that Hopf bifurcation is still possible as  $\varepsilon \rightarrow 0$  as long as (i)  $\sigma \rightarrow 0$  as well and (ii)  $(\sigma, \varepsilon) = (0, 0)$  is approached from the interior of the red region.

More generally, Figure 2 shows that the qualitative dynamics of system (54) as  $(\sigma, \varepsilon) \rightarrow (0, 0)$  depends in an important way on how the point  $(0, 0)$  is approached, i.e. on the path in  $(\sigma, \varepsilon)$ -space along which the limit is taken. This is a subtle but important point, because it shows that the relative size of the small parameters  $\varepsilon$  and  $\sigma$  (and not only the fact that both  $\varepsilon \rightarrow 0$  and  $\sigma \rightarrow 0$ ) plays an important role in determining the qualitative dynamics of the model.

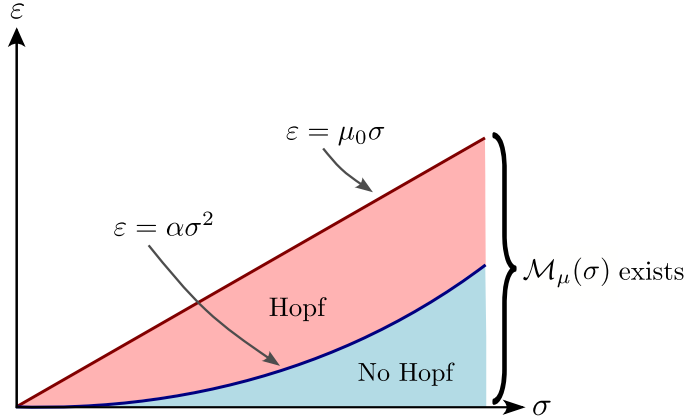


Figure 2: The positive quadrant of the  $(\sigma, \varepsilon)$ -plane is shown. The line  $\varepsilon = \mu_0\sigma$ , i.e.  $\mu = \mu_0$ , defines a boundary below which our first main result (Theorem 1.2 assertion 1) guarantees the existence of  $\mathcal{M}_\mu(\sigma)$ . The quadratic curve  $\varepsilon = \alpha\sigma^2$  in dark blue divides the region defined by  $0 < \varepsilon < \mu_0\sigma$  into two distinct (asymptotic) subregions. Hopf bifurcations are possible (impossible) in the red (blue) subregion; see assertion 2 of Theorem 1.2 and the discussion in the text for details.

In order to prove Theorem 1.2, we follow [26, Section 8], which uses blow-up to analyse regularized PWS systems with intersecting discontinuity sets. We also refer to [28, 30, 31, 32, 40] for earlier work on the use of blow-up for regularized PWS systems and to [24, 33, 44, 48] for its use in applications. In particular, we first consider the extended system obtained after appending the trivial equation  $\sigma' = 0$  to system (4) <sub>$\varepsilon=\mu\sigma$</sub> , recall (10). This system loses smoothness along  $(r_a, r_b, p_a, p_b, \sigma) \in \Sigma \times \{0\}$ , but we gain smoothness after applying a sequence of transformations that blow up  $\Sigma \times \{0\}$ ; the result is illustrated schematically in Figure 3 using a projection onto  $(p_a, p_b, \sigma)$ -space. For the specific form of the blow-up transformations in the context of system (4), we draw inspiration from the MSc thesis [13], where the planar “fundamental problem” from [45] was analysed.

We will show that the QSSR constraint in (7) defines a normally hyperbolic and attracting critical manifold  $\overline{\mathcal{M}}$  for  $\mu = 0$  on the blown up space obtained after consecutive blow-ups. We emphasise that this fact relies upon the scaling (10). In this way, we obtain a locally invariant slow manifold  $\overline{\mathcal{M}}_\mu$  for all  $0 < \mu < \mu_0$  by Fenichel’s coordinate-independent theory for normally hyperbolic invariant manifolds (see [11, Thm. 9.1] in particular), and finally  $\mathcal{M}_\mu(\sigma)$  in Theorem 1.2 upon the process of ‘blowing down’ to the original  $(r_a, r_b, p_a, p_b)$ -space. As stated, the perturbed manifold  $\mathcal{M}_\mu(\sigma)$  is  $C^0$   $\mathcal{O}(\mu)$ -close to the QSSR manifold defined via (7), uniformly with respect to  $\sigma > 0$ . Higher order  $C^k$ -closeness is not possible (globally) as the derivatives become unbounded with respect to  $\sigma \rightarrow 0$ . This should be clear enough from the dependency of  $\sigma^{-1}$  in the equations for  $r_a$  and  $r_b$  in system (4). However, these unbounded derivatives are ‘tamed’ in our blow-up coordinates. At the same time, the blow up as  $\sigma \rightarrow 0$  is only relevant near  $\Sigma$ ; away from these sets we have  $C^k$ -closeness (in agreement with the statement in Remark 1.4).

Once we have proven Theorem 1.2, we show how the results can be used for further analytical and numerical investigations of the dynamics of system (4). Although we focus entirely on the dynamics of a simple, 4-dimensional GRN model, our results suggest that the dynamics of high-dimensional GRN systems in the general form (1) may depend in an important way on the relative size of  $\varepsilon$  and the small parameters  $1/n_i$  associated with switching effects. The question of whether and how our results can be extended to the study of the generally high-dimensional network (1) is the topic of on-going work. We are hopeful that a geometric blow-up based approach will provide a means to study the effects of both (i) and (ii) in a single, geometrically informative and rigorous mathematical framework.

## 1.4 Overview

The remainder of the paper is structured as follows: In Section 2, we present the blow-up construction. In particular, we demonstrate (by working in local coordinate charts) that (7) defines an attracting and normally hyperbolic critical manifold for  $\mu = 0$  on a blown-up space. Section 3 is devoted to the proof

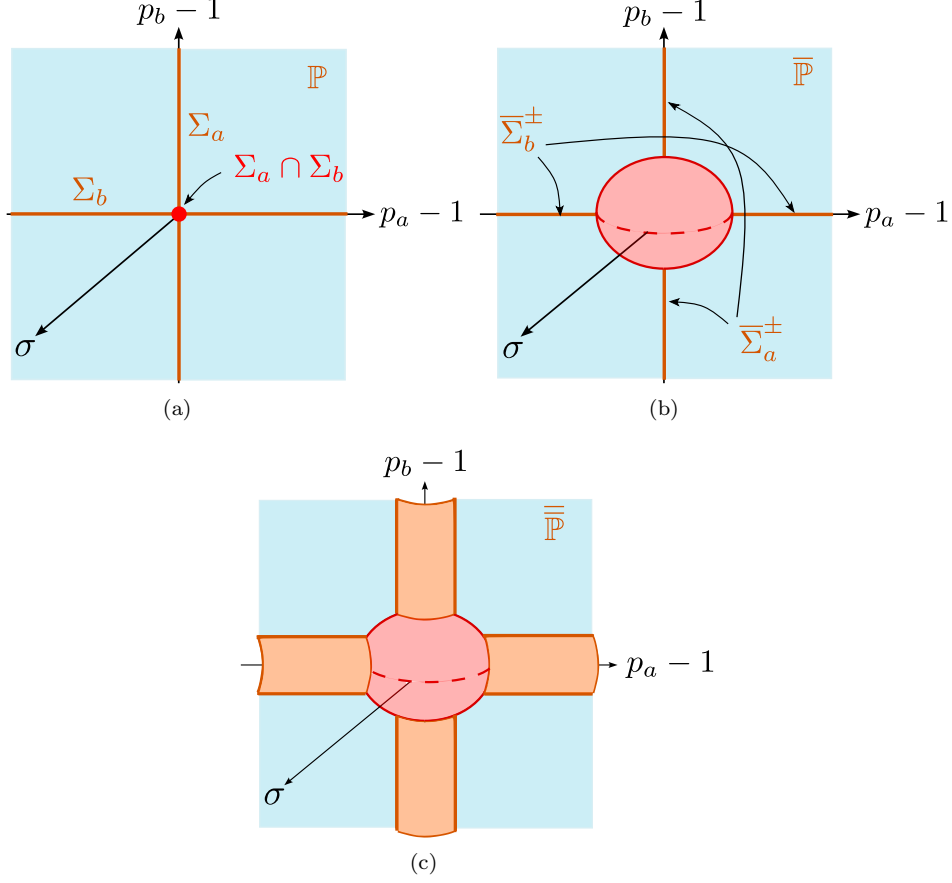


Figure 3: Schematic representation of the sequence of blow-up transformations which allow us to resolve the loss of smoothness along the singular set  $\Sigma_a \cup \Sigma_b$  in system (4) when  $\sigma = 0$ . In (a),  $\Sigma_a$  and  $\Sigma_b$  are illustrated (as projections) within the  $(p_a, p_b)$ -plane. To resolve the lack of smoothness, we first resolve the intersection  $\Sigma_a \cap \Sigma_b$  (red) with a spherical blow-up transformation. This gives the intermediate blown-up space  $\bar{\mathbb{P}}$  in (b). Subsequently, we blow-up the remaining singularities  $\bar{\Sigma}_b^\pm$  and  $\bar{\Sigma}_a^\pm$  along the axes, using cylindrical blow-ups. This gives the final blown up space  $\bar{\bar{\mathbb{P}}}$  in (c).

of Theorem 1.2. In Section 4 we use Theorem 1.2 for further analytical and numerical investigations of the dynamics of system (4) by using numerical computations and our reduction in Theorem 1.2, thereby demonstrating the applicability of our results. We conclude with a summary and outlook in Section 5.

**Remark 1.6.** *We have decided to present the geometric blow-up and proof of Theorem 1.2 in Sections 2-3, since we consider the mathematical techniques, rather than the dynamics of system (4) per se, to be the primary contribution of this work. Nevertheless, efforts have been made in order to ensure that the reader who is primarily interested in the dynamics of system (4) can skip directly to Section 4.*

## 2 Blow-up

In order to prove assertion 1 of Theorem 1.2, we consider the extended system

$$\begin{aligned}
 r'_a &= \phi(\sigma^{-1} \log p_b) - r_a, \\
 r'_b &= 1 - \phi(\sigma^{-1} \log p_a) - \gamma r_b, \\
 p'_a &= \mu \sigma p_a G_a(r_a, \log p_a), \\
 p'_b &= \mu \sigma p_b G_b(r_b, \log p_b), \\
 \sigma' &= 0,
 \end{aligned} \tag{12}$$

which is obtained from system (4) with  $\varepsilon = \mu\sigma$  after appending the trivial equation  $\sigma' = 0$ . Here we have also simplified the expressions for the Hill functions by defining

$$\phi(x) := \frac{e^x}{1 + e^x}, \quad (13)$$

and introducing

$$G_a(x, y) := \xi_a x e^{-y} - 1, \quad G_b(x, y) := \delta(\xi_b x e^{-y} - 1). \quad (14)$$

This will help to simplify the notation in charts below. In fact, assertion 1 of Theorem 1.2 holds true for any smooth functions  $G_a$  and  $G_b$ . Only assertions 2–3 use (14). The system (12) loses smoothness along  $\Sigma \times \{0\}$ , recall (8) and (9). In the following, we will resolve this lack of smoothness through blow-up and show that the QSSR constraints

$$r_a = \phi(\sigma^{-1} \log p_b), \quad r_b = \gamma^{-1}(1 - \phi(\sigma^{-1} \log p_a)), \quad (15)$$

when written in the blown-up space, define an attracting and normally hyperbolic critical manifold for  $\mu = 0$ .

## 2.1 Spherical blow-up along the intersection $\Sigma_a \cap \Sigma_b$

First, we resolve the most degenerate set  $(\Sigma_a \cap \Sigma_b) \times \{0\} \subset \Sigma \times \{0\}$ , corresponding to  $(p_a, p_b, \sigma) = (1, 1, 0)$ , by blowing it up to a ‘cylinder of spheres’. In particular, we define

$$\mathbb{P} := \{(r_a, r_b, p_a, p_b, \sigma) : r_a, r_b, p_a, p_b, \sigma \geq 0\},$$

so that  $\mathbb{P} \setminus \Sigma$  is the phase-space of system (12), and write

$$\bar{\mathbb{P}} := \{(r_a, r_b, \eta, (\bar{u}, \bar{v}, \bar{\sigma})) : r_a, r_b, \eta \geq 0, (\bar{u}, \bar{v}, \bar{\sigma}) \in \mathbb{H}^2\},$$

where

$$\mathbb{H}^2 := \{(\bar{u}, \bar{v}, \bar{\sigma}) \in \mathbb{R}^3 : \bar{u}^2 + \bar{v}^2 + \bar{\sigma}^2 = 1, \bar{\sigma} \geq 0\}$$

is the  $\bar{\sigma} \geq 0$ -hemisphere of the sphere  $\mathbb{S}^2$ . Then, following [13], the relevant blow-up transformation  $\bar{\Phi} : \mathbb{P} \rightarrow \bar{\mathbb{P}}$  fixes  $r_a$  and  $r_b$  and takes

$$(\eta, (\bar{u}, \bar{v}, \bar{\sigma})) \mapsto \begin{cases} p_a = e^{\eta \bar{u}}, \\ p_b = e^{\eta \bar{v}}, \\ \sigma = \eta \bar{\sigma}, \end{cases} \quad \eta \geq 0, (\bar{u}, \bar{v}, \bar{\sigma}) \in \mathbb{H}^2. \quad (16)$$

Therefore the pre-image of  $(\Sigma_a \cap \Sigma_b) \times \{0\}$  under  $\bar{\Phi}$  is  $r_a, r_b \geq 0, \eta = 0, (\bar{u}, \bar{v}, \bar{\sigma}) \in \mathbb{H}^2$ . Notice also that under the substitution of (16), the defining equations for the QSSR manifold in (7) become

$$r_a = \phi(\bar{v} \bar{\sigma}^{-1}), \quad r_b = \gamma^{-1}(1 - \phi(\bar{u} \bar{\sigma}^{-1})), \quad (17)$$

which are well-defined for  $(\bar{u}, \bar{v}, \bar{\sigma}) \in \mathbb{H}^2 \cap \{\bar{\sigma} > 0\}$ . In fact, (17) has a well-defined smooth extension to the equator circle  $\mathbb{H}^2 \cap \{\bar{\sigma} = 0\}$  away from the degenerate points  $(\bar{u}, \bar{v}, \bar{\sigma}) = (\pm 1, 0, 0), (0, \pm 1, 0)$  defined by

$$r_a = \begin{cases} 1 & \bar{v} > 0, \bar{\sigma} = 0, \\ 0 & \bar{v} < 0, \bar{\sigma} = 0, \end{cases} \quad r_b = \begin{cases} 0 & \bar{u} > 0, \bar{\sigma} = 0, \\ \gamma^{-1} & \bar{u} < 0, \bar{\sigma} = 0. \end{cases}$$

Here we have used the definition (13). We therefore define the corresponding degeneracies as subsets of  $\bar{\mathbb{P}}$ :

$$\bar{\Sigma} = \bigcup_{\substack{i \in \{a, b\} \\ j \in \{\pm\}}} \bar{\Sigma}_i^j,$$

where

$$\begin{aligned} \bar{\Sigma}_a^\pm &= \{(r_a, r_b, \eta, (\bar{u}, \bar{v}, \bar{\sigma})) \in \bar{\mathbb{P}} : (\bar{u}, \bar{v}, \bar{\sigma}) = (\pm 1, 0, 0)\}, \\ \bar{\Sigma}_b^\pm &= \{(r_a, r_b, \eta, (\bar{u}, \bar{v}, \bar{\sigma})) \in \bar{\mathbb{P}} : (\bar{u}, \bar{v}, \bar{\sigma}) = (0, \pm 1, 0)\}, \end{aligned}$$

respectively. Now, let  $X$  denote the vector-field defined by system (12) on  $\mathbb{P} \setminus \Sigma$ . In Section 2.1.1, we will show that the pull-back vector-field

$$\bar{X} := \Phi^*(X),$$

is well-defined on

$$\bar{\mathbb{P}} \setminus \bar{\Sigma}, \quad (18)$$

and that (17) defines an attracting and normally hyperbolic critical submanifold  $\bar{\mathcal{M}}$  of (18) for  $\mu = 0$ . For this purpose, we will work with an atlas consisting of five different coordinate charts, defined projectively via

$$K_1 : \bar{u} = -1, \quad K_2 : \bar{\sigma} = 1, \quad K_3 : \bar{u} = 1, \quad K_4 : \bar{v} = -1, \quad K_5 : \bar{v} = 1.$$

We introduce local coordinates in each chart as follows:

$$\begin{aligned} K_1 : (p_a, p_b, \sigma) &= (e^{-\eta_1}, e^{\eta_1 v_1}, \eta_1 \sigma_1), \\ K_2 : (p_a, p_b, \sigma) &= (e^{\eta_2 u_2}, e^{\eta_2 v_2}, \eta_2), \\ K_3 : (p_a, p_b, \sigma) &= (e^{\eta_3}, e^{\eta_3 v_3}, \eta_3 \sigma_3), \\ K_4 : (p_a, p_b, \sigma) &= (e^{\eta_4 u_4}, e^{-\eta_4}, \eta_4 \sigma_4), \\ K_5 : (p_a, p_b, \sigma) &= (e^{\eta_5 u_5}, e^{\eta_5}, \eta_5 \sigma_5), \end{aligned} \quad (19)$$

where all  $\eta_i \geq 0$ ,  $\sigma_i \geq 0$ ,  $u_i \in \mathbb{R}$ ,  $v_i \in \mathbb{R}$ . Diffeomorphic change of coordinate maps between overlapping coordinate charts can be derived using these expressions. Given that there is a large number of them, we do not state them explicitly here.

### 2.1.1 Analysis in charts $K_i$

The equations in the scaling chart  $K_2$  are given by

$$\begin{aligned} r'_a &= \phi(v_2) - r_a, \\ r'_b &= 1 - \phi(u_2) - \gamma r_b, \\ u'_2 &= \mu G_a(r_a, \eta_2 u_2), \\ v'_2 &= \mu G_b(r_b, \eta_2 v_2), \\ \eta'_2 &= 0. \end{aligned} \quad (20)$$

This is the local form  $X_2$  of  $\bar{X}$  in chart  $K_2$ . System (20) is smooth and slow-fast in standard form with respect to  $\mu \rightarrow 0$ , depending regularly upon  $\eta_2 = \sigma \geq 0$ . In particular, the local form  $\mathcal{M}_2$  of  $\bar{\mathcal{M}}$ , defined by

$$r_a = \phi(v_2), \quad r_b = \gamma^{-1}(1 - \phi(u_2)), \quad (21)$$

is an attracting and normally hyperbolic critical manifold of (20)| $_{\mu=0}$  with nontrivial eigenvalues  $-1$  and  $-\gamma < 0$ . We will use the following result later on.

**Lemma 2.1.** *Fix any  $k \in \mathbb{N}$ ,  $\eta_{20} > 0$ , and any compact connected domain  $K_2 \subset \mathbb{R}^2$ . There exists a  $\mu_0 > 0$  such that the compact submanifold  $\mathcal{M}_{0,2} \subset \mathcal{M}_2$ , defined by (21) and  $(u_2, v_2) \in K_2$ , persists as a locally invariant attracting  $C^k$ -smooth slow manifold  $\mathcal{M}_{\mu,2}$  of the graph form*

$$\begin{aligned} r_a &= \phi(v_2) + \mu \Omega_a(u_2, v_2, \eta_2) + \mathcal{O}(\mu^2), \\ r_b &= 1 - \phi(u_2) + \mu \Omega_b(u_2, v_2, \eta_2) + \mathcal{O}(\mu^2), \end{aligned} \quad (22)$$

for  $(u_2, v_2) \in K_2$ ,  $\eta_2 \in [0, \eta_{20}]$  and all  $\mu \in [0, \mu_0)$ . In particular,

$$\begin{aligned} \Omega_a(u_2, v_2, \eta_2) &= -\delta \phi(v_2)(1 - \phi(v_2))G_b(\gamma^{-1}(1 - \phi(u_2)), \eta_2 v_2), \\ \Omega_b(u_2, v_2, \eta_2) &= \gamma^{-2} \phi(u_2)(1 - \phi(u_2))G_a(\phi(v_2), \eta_2 u_2), \end{aligned} \quad (23)$$

and the  $\mathcal{O}(\mu^2)$ -terms are all  $C^k$ -smooth with respect to  $(u_2, v_2) \in K_2$ ,  $\eta_2 \in [0, \eta_{20}]$ , and  $\mu \in [0, \mu_0)$ .

*Proof.* The existence of  $\mathcal{M}_{\mu,2}$  follows directly from Fenichel theory, see e.g. [25, Thm. 2]. The expansions in (22) and (23) are consequences of simple calculations, the details of which we leave out for simplicity.  $\square$

Since the equations in the phase-directional charts  $K_1$ ,  $K_3$ ,  $K_4$  and  $K_5$  have a similar algebraic structure, we shall consider them simultaneously. In order to do so, we introduce the following additional notation:

$$s_i = \begin{cases} +1 & \text{if } i \in \{3, 5\}, \\ -1 & \text{if } i \in \{1, 4\}. \end{cases}$$

This allows us to write the equations in  $K_1$  and  $K_3$  collectively as

$$\begin{aligned} r'_a &= \phi(v_i \sigma_i^{-1}) - r_a, \\ r'_b &= 1 - \phi(s_i \sigma_i^{-1}) - \gamma r_b, \\ \eta'_i &= \mu s_i \eta_i \sigma_i G_a(r_a, s_i \eta_i), \\ v'_i &= \mu \sigma_i [G_b(r_b, \eta_i v_i) - s_i v_i G_a(r_a, s_i \eta_i)], \\ \sigma'_i &= -\mu s_i \sigma_i^2 G_a(r_a, s_i \eta_i), \end{aligned} \tag{24}$$

where  $i \in \{1, 3\}$  is the index associated with the coordinate chart  $K_i$ . Similarly, we can write the equations in  $K_4$  and  $K_5$  collectively as

$$\begin{aligned} r'_a &= \phi(s_i \sigma_i^{-1}) - r_a, \\ r'_b &= 1 - \phi(u_i \sigma_i^{-1}) - \gamma r_b, \\ u'_i &= \mu \sigma_i [G_a(r_a, \eta_i u_i) - s_i u_i G_b(r_b, s_i \eta_i)], \\ \eta'_i &= \mu s_i \eta_i \sigma_i G_b(r_b, s_i \eta_i), \\ \sigma'_i &= -\mu s_i \sigma_i^2 G_b(r_b, s_i \eta_i), \end{aligned} \tag{25}$$

where  $i \in \{4, 5\}$ . These are the local forms  $X_i$  of  $\bar{X}$  in the charts  $K_i$ ,  $i \in \{1, 3, 4, 5\}$ , respectively.  $X_1$  and  $X_3$  (given by (24)) are smooth everywhere except along the 3-dimensional hyperplanes

$$\Sigma_{b,i} = \{(r_a, r_b, \eta_i, 0, 0) : r_a, r_b, \eta_i \geq 0\},$$

defined by  $v_i = \sigma_i = 0$  for  $i \in \{1, 3\}$ , respectively; these sets are the local versions of  $\bar{\Sigma}_b^\pm$  and correspond to the left and right branches of  $\Sigma_b \times \{0\}$  after blow-down (i.e. upon application of the map  $\bar{\Phi}$ ) respectively, see Figure 3 (a) and (b). Moreover, away from  $\Sigma_{b,i}$  the local versions  $\mathcal{M}_{i,0}$ ,  $i \in \{1, 3\}$ , of  $\mathcal{M}$ , defined by

$$r_a = \phi(v_i \sigma_i^{-1}), \quad r_b = \gamma^{-1}(1 - \phi(s_i \sigma_i^{-1})),$$

are attracting and normally hyperbolic critical manifolds of (24) with nontrivial eigenvalues  $-1$  and  $-\gamma < 0$ .

Similarly,  $X_4$  and  $X_5$  (given by (25)) are smooth everywhere except along the 3-dimensional hyperplanes

$$\Sigma_{a,i} = \{(r_a, r_b, 0, \eta_i, 0) : r_a, r_b, \eta_i \geq 0\},$$

defined by  $u_i = \sigma_i = 0$  for  $i \in \{4, 5\}$ , respectively; these sets are the local versions of  $\bar{\Sigma}_a^\pm$  and correspond to the lower and upper branches of  $\Sigma_a \times \{0\}$  after blow-down respectively. We refer again to Figure 3 (a) and (b). Finally, away from  $\Sigma_{a,i}$  the local versions  $\mathcal{M}_i$ ,  $i \in \{4, 5\}$ , of  $\mathcal{M}$ , defined by

$$r_a = \phi(s_i \sigma_i^{-1}), \quad r_b = \gamma^{-1}(1 - \phi(u_i \sigma_i^{-1})),$$

are attracting and normally hyperbolic critical manifolds of (25) with nontrivial eigenvalues  $-1$  and  $-\gamma < 0$ .

## 2.2 Cylindrical blow-ups along $\bar{\Sigma}$

We now turn to the remaining degeneracies along  $\bar{\Sigma}$ . Consider first the subsets  $\bar{\Sigma}_b^\pm \subset \bar{\Sigma}$  and define the following sets

$$\bar{\mathbb{P}}_b^\pm := \bar{\mathbb{P}} \cap \{\bar{u} \geq 0\},$$

respectively, and

$$\bar{\mathbb{Q}} := \{(r_a, r_b, \eta, \rho, (\bar{u}, \bar{\sigma})) : r_a, r_b, \eta, \rho \geq 0, (\bar{v}, \bar{\sigma}) \in \mathbb{H}^1\},$$

where

$$\mathbb{H}^1 := \{(\bar{v}, \bar{\sigma}) \in \mathbb{R}^2 : \bar{v}^2 + \bar{\sigma}^2 = 1, \bar{\sigma} \geq 0\}$$

is the  $\bar{\sigma} \geq 0$  half of the unit circle  $\mathbb{S}^1$ . Now we apply the blow-up transformations  $\bar{\Phi}_b^\pm : \bar{\mathbb{Q}} \rightarrow \bar{\mathbb{P}}_b^\pm$ , which fix  $r_a, r_b, \eta$  and take

$$(\rho, (\bar{u}, \bar{\sigma})) \mapsto \begin{cases} \bar{v}\bar{u}^{-1} = \pm\rho\bar{v}, \\ \bar{\sigma}\bar{u}^{-1} = \pm\rho\bar{\sigma}, \end{cases} \quad \rho \geq 0, (\bar{v}, \bar{\sigma}) \in \mathbb{H}^1, \quad (26)$$

respectively. The preimages of  $\bar{\Sigma}_b^\pm$  under  $\bar{\Phi}_b^\pm$  are the cylinders defined by  $\bar{\mathbb{Q}} \cap \{\rho = 0\}$ . Notice also that under the substitutions of (26), the QSSR constraints in (17) become

$$r_a = \phi(\bar{v}\bar{\sigma}^{-1}), \quad r_b = \gamma^{-1}(1 - \phi(\rho^{-1}\bar{\sigma}^{-1})), \quad (27)$$

respectively. There are two cases, corresponding to  $\pm$ , and they are both well-defined on  $\bar{\mathbb{Q}}$ . Indeed, in polar coordinates  $(\bar{v}, \bar{\sigma}) = (\cos \nu, \sin \nu)$ ,  $\nu \in [0, \pi]$ , we have

$$\phi(\bar{v}\bar{\sigma}^{-1}) = \begin{cases} 1 & \text{if } \nu = 0 \\ \frac{e^{\cot \nu}}{1+e^{\cot \nu}} & \text{if } \nu \in (0, \pi), \\ 0 & \text{if } \nu = \pi \end{cases}, \quad \phi(-\bar{v}\bar{\sigma}^{-1}) = \begin{cases} 0 & \text{if } \nu = 0 \\ \frac{e^{-\cot \nu}}{1+e^{-\cot \nu}} & \text{if } \nu \in (0, \pi), \\ 1 & \text{if } \nu = \pi \end{cases},$$

respectively. These expressions are  $C^\infty$ -flat at the end points  $\nu = 0$  and  $\nu = \pi$ .

The degeneracies along  $\bar{\Sigma}_a^\pm$  are handled in the same way. First, we define

$$\bar{\mathbb{P}}_a^\pm := \bar{\mathbb{P}} \cap \{\bar{v} \geq 0\},$$

and apply the blow-up transformations  $\bar{\Phi}_a^\pm : \bar{\mathbb{Q}} \rightarrow \bar{\mathbb{P}}_a^\pm$  which fix  $r_a, r_b, \eta$  and take

$$(\rho, (\bar{u}, \bar{\sigma})) \mapsto \begin{cases} \bar{u}\bar{v}^{-1} = \pm\rho\bar{u}, \\ \bar{\sigma}\bar{v}^{-1} = \pm\rho\bar{\sigma}, \end{cases} \quad \rho \geq 0, (\bar{u}, \bar{\sigma}) \in \mathbb{H}^1, \quad (28)$$

respectively. Under the substitutions of (28), the QSSR constraints in (17) become

$$r_a = \phi(\rho^{-1}\bar{\sigma}^{-1}), \quad r_b = \gamma^{-1}(1 - \phi(\bar{u}\bar{\sigma}^{-1})), \quad (29)$$

respectively. There are again two cases, corresponding to  $\pm$ , and they are both well-defined on  $\bar{\mathbb{Q}}$ , including on the cylinder  $\bar{\mathbb{Q}} \cap \{\rho = 0\}$  which corresponds to the blow-up of  $\bar{\Sigma}_a^\pm$  by the inverse process of  $\bar{\Phi}_a^\pm$ .

In Sections 2.3 and 2.4, we will show that the pull-back vector-fields

$$\bar{X}_b^\pm = (\bar{\Phi}_b^\pm)^*(\bar{X}|_{\bar{\mathbb{P}}_b^\pm}), \quad \bar{X}_a^\pm = (\bar{\Phi}_a^\pm)^*(\bar{X}|_{\bar{\mathbb{P}}_a^\pm}),$$

have well-defined smooth extensions to  $\bar{\mathbb{Q}} \cap \{\rho = 0\}$ . Moreover, we will show that (27) and (29) define attracting and normally hyperbolic critical manifolds  $\bar{\mathcal{M}}_b^\pm$  and  $\bar{\mathcal{M}}_a^\pm$  of  $\bar{X}_b^\pm$  and  $\bar{X}_a^\pm$ , respectively. For

this purpose, we define atlases of local charts. Notice first that in the charts  $K_i$ ,  $i \in \{1, 3\}$ , which cover  $\overline{\mathbb{P}}_b^\pm$ , the transformations (26) take the local forms

$$(\rho, (\bar{v}, \bar{\sigma})) \mapsto \begin{cases} v_i = \rho \bar{v}, \\ \sigma_i = \rho \bar{\sigma}, \end{cases} \quad i \in \{1, 3\},$$

respectively. We therefore introduce 6 local coordinate charts which cover the three sides  $\bar{\sigma} > 0$ ,  $\bar{v} \leq 0$  of each branch of the left (when  $i = 1$ ) and right (when  $i = 3$ ) blow-up cylinders in Figure 3 (c); see also Figure 4. We define them via

$$K_{i2} : \bar{\sigma}_i = 1, \quad K_{i4} : \bar{v}_i = -1, \quad K_{i5} : \bar{v}_i = 1,$$

respectively, and write the local coordinates as

$$\begin{aligned} K_{i2} : (v_i, \sigma_i) &= (\rho_{i2} v_{i2}, \rho_{i2}), \\ K_{i4} : (v_i, \sigma_i) &= (-\rho_{i4}, \rho_{i4} \sigma_{i4}), \\ K_{i5} : (v_i, \sigma_i) &= (\rho_{i3}, \rho_{i5} \sigma_{i5}), \end{aligned} \quad (30)$$

where all  $\rho_{ij} \geq 0$ ,  $\sigma_{ij} \geq 0$ ,  $v_{i2} \in \mathbb{R}$ . By composing (30) with (19), we can also write the local coordinates in terms of the original variables  $(p_a, p_b, \sigma)$  as follows:

$$\begin{aligned} K_{i2} : (p_a, p_b, \sigma) &= (e^{s_i \eta_i}, e^{\eta_i \rho_{i2} v_{i2}}, \eta_i \rho_{i2}), \\ K_{i4} : (p_a, p_b, \sigma) &= (e^{s_i \eta_i}, e^{-\eta_i \rho_{i4}}, \eta_i \rho_{i4} \sigma_{i4}), \\ K_{i5} : (p_a, p_b, \sigma) &= (e^{s_i \eta_i}, e^{\eta_i \rho_{i5}}, \eta_i \rho_{i5} \sigma_{i5}). \end{aligned} \quad (31)$$

We proceed analogously for  $\overline{\mathbb{P}}_a^\pm$ . First, we notice that in the charts  $K_i$ ,  $i \in \{4, 5\}$ , which cover  $\overline{\mathbb{P}}_a^\pm$ , the transformations (28) take the local forms

$$(\rho, (\bar{u}, \bar{\sigma})) \mapsto \begin{cases} u_i = \rho \bar{u}, \\ \sigma_i = \rho \bar{\sigma}, \end{cases} \quad i \in \{4, 5\},$$

respectively. We again work in 6 local coordinate charts, which cover the three sides  $\bar{\sigma} > 0$ ,  $\bar{u} \leq 0$  of each branch of the bottom (when  $i = 4$ ) and top (when  $i = 5$ ) blow-up cylinders emanating from the blow-up sphere in Figure 3 (c); see also Figure 4. We define them via

$$K_{i1} : \bar{u}_i = -1, \quad K_{i2} : \bar{\sigma}_i = 1, \quad K_{i3} : \bar{u}_i = 1,$$

respectively, and write the local coordinates as

$$\begin{aligned} K_{i1} : (u_i, \sigma_i) &= (-\rho_{i1}, \rho_{i1} \sigma_{i1}), \\ K_{i2} : (u_i, \sigma_i) &= (\rho_{i2} u_{i2}, \rho_{i2}), \\ K_{i3} : (u_i, \sigma_i) &= (\rho_{i3}, \rho_{i3} \sigma_{i3}), \end{aligned} \quad (32)$$

where all  $\rho_{ij} \geq 0$ ,  $\sigma_{ij} \geq 0$ ,  $u_{i2} \in \mathbb{R}$ . By composing (32) with (19), we can also write the local coordinates in terms of the original variables  $(p_a, p_b, \sigma)$  as follows:

$$\begin{aligned} K_{i1} : (p_a, p_b, \sigma) &= (e^{-\eta_i \rho_{i1}}, e^{s_i \eta_i}, \eta_i \rho_{i1} \sigma_{i1}), \\ K_{i2} : (p_a, p_b, \sigma) &= (e^{\eta_i \rho_{i2} u_{i2}}, e^{s_i \eta_i}, \eta_i \rho_{i2}), \\ K_{i3} : (p_a, p_b, \sigma) &= (e^{\eta_i \rho_{i3}}, e^{s_i \eta_i}, \eta_i \rho_{i3} \sigma_{i3}). \end{aligned} \quad (33)$$

**Remark 2.2.** *The subscript notation here and throughout this section has been chosen so that the subscripts/indices 1 and 3 are associated with ' $\bar{u} = \pm 1$ ', whereas the subscripts/indices '4' and '5' are associated with ' $\bar{v} = \pm 1$ '. For clarity, this is sketched in Figure 4.*

In combination,  $\overline{\overline{\mathbb{P}}}_b^\pm$  and  $\overline{\overline{\mathbb{P}}}_a^\pm$  blow up  $\overline{\mathbb{P}}$  to our final blown up space  $\overline{\overline{\mathbb{P}}}$ , which has been illustrated in Figures 3 (c) and 4. The 13 charts given by

$$K_2, \quad \{K_{ij} : i \in \{1, 3\}, j \in \{2, 4, 5\}\} \quad \text{and} \quad \{K_{ij} : i \in \{4, 5\}, j \in \{1, 2, 3\}\}, \quad (34)$$

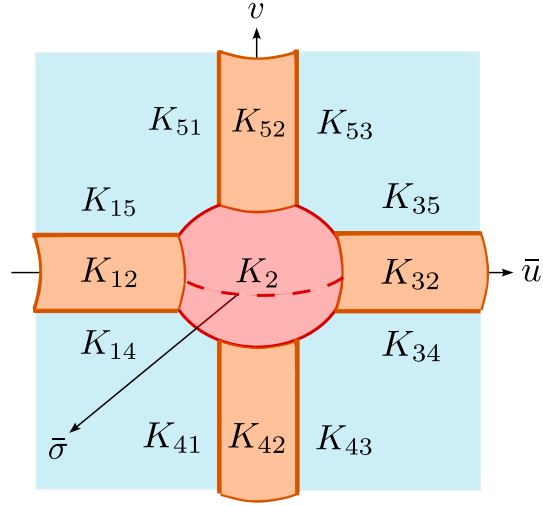


Figure 4: Schematic representation of the regions in  $(\bar{u}, \bar{v}, \bar{\sigma})$ -space that are covered by the rescaling chart  $K_2$  and the 12 coordinate charts  $K_{ij}$  defined in the text; see also Remark 2.2. These 13 coordinate charts are used in order to cover the (complete) blown-up space.

see (19), (30), (32) and Figure 4, provide an atlas of  $\bar{\mathbb{P}}$ . Diffeomorphic change of coordinate maps between overlapping coordinate charts can be derived using (19), (31) and (33). For simplicity, we only show the changes of coordinates  $\kappa_{2,ij} : K_2 \rightarrow K_{ij}$ , from  $K_2$  to  $K_{ij}$ ,  $i \in \{1, 3\}$ ,  $j \in \{2, 4, 5\}$ :

$$\begin{aligned} \kappa_{2,i2} : (\eta_2, u_2, v_2) &\mapsto \begin{cases} \eta_i = s_i \eta_2 u_2, \\ \rho_{i2} = s_i u_2^{-1}, & v_2 \in \mathbb{R}, \quad s_i u_2 > 0, \\ v_{i2} = v_2, \end{cases} \\ \kappa_{2,i4} : (\eta_2, u_2, v_2) &\mapsto \begin{cases} \eta_i = s_i \eta_2 u_2, \\ \rho_{i4} = -s_i v_2 u_2^{-1}, & v_2 < 0, \quad s_i u_2 > 0, \\ \sigma_{i4} = -v_2^{-1}, \end{cases} \\ \kappa_{2,i5} : (\eta_2, u_2, v_2) &\mapsto \begin{cases} \eta_i = s_i \eta_2 u_2, \\ \rho_{i5} = s_i v_2 u_2^{-1}, & v_2 > 0, \quad s_i u_2 > 0. \\ \sigma_{i5} = v_2^{-1} \end{cases} \end{aligned}$$

Here we have also emphasized where these mappings are well-defined.

### 2.3 Analysis in the charts $K_{ij}$ used to cover the blow-up of $\bar{\Sigma}_b$

We now consider the equations in charts  $K_{ij}$  with  $(i, j) \in \{1, 3\} \times \{2, 4, 5\}$ , which cover the blow-up of  $\bar{\Sigma}_b$ . The equations in the charts  $K_{i2}$  are given by

$$\begin{aligned} r'_a &= \phi(v_{i2}) - r_a, \\ r'_b &= 1 - \phi(s_i \rho_{i2}^{-1}) - \gamma r_b, \\ \eta'_i &= \mu s_i \eta_i \rho_{i2} G_a(r_a, s_i \eta_i), \\ v'_{i2} &= \mu G_b(r_b, \rho_{i2} \eta_i v_{i2}), \\ \rho'_{i2} &= -\mu s_i \rho_{i2}^2 G_a(r_a, s_i \eta_i), \end{aligned} \tag{35}$$

with  $\eta_i \geq 0$ ,  $\rho_{i2} \geq 0$ . Both of the systems defined by (35) (corresponding to  $i \in \{1, 3\}$ ) are smooth and slow-fast with respect to  $\mu \rightarrow 0$ . Notice in particular that  $\phi(s_i \rho_{i2}^{-1})$ ,  $\rho_{i2} > 0$ , extends smoothly to  $\rho_{i2} = 0$  since

$$\lim_{\rho_{i2} \rightarrow 0} \phi(s_i \rho_{i2}^{-1}) = \begin{cases} 0 & \text{if } i = 1, \\ 1 & \text{if } i = 3. \end{cases}$$

Here we have also used (13). Therefore the local versions  $\mathcal{M}_{b,i2}$  of  $\overline{\mathcal{M}}_b$ , defined by

$$r_a = \phi(v_{i2}), \quad r_b = \gamma^{-1}(1 - \phi(s_i \rho_{i2}^{-1})),$$

are 3-dimensional attracting and normally critical manifolds of (35) for  $\mu = 0$  with non-trivial eigenvalues  $-1$  and  $-\gamma < 0$ .

The equations in the charts  $K_{i4}$  and  $K_{i5}$  are given by

$$\begin{aligned} r'_a &= \phi(m_j \sigma_{ij}^{-1}) - r_a, \\ r'_b &= 1 - \phi(s_i (\rho_{ij} \sigma_{ij})^{-1}) - \gamma r_b, \\ \eta'_i &= \mu s_i \eta_i \rho_{ij} \sigma_{ij} G_a(r_a, s_i \eta_i), \\ \rho'_{ij} &= \mu m_j \rho_{ij} \sigma_{ij} [G_b(r_b, m_j \rho_{ij} \eta_i) - s_i m_j \rho_{ij} G_a(r_a, s_i \eta_i)], \\ \sigma'_{ij} &= -\mu m_j \sigma_{ij}^2 G_b(r_b, m_j \rho_{ij} \eta_i), \end{aligned} \tag{36}$$

with  $\rho_{ij} \geq 0$ ,  $\sigma_{ij} \geq 0$ ,  $(i, j) \in \{1, 3\} \times \{4, 5\}$ , and

$$m_j = \begin{cases} -1 & \text{if } j = 4, \\ 1 & \text{if } j = 5. \end{cases}$$

The equations in (36) define four different systems (since there are four distinct couples  $\{i, j\}$ ), each of which are smooth slow-fast systems with respect to  $\mu \rightarrow 0$ . Notice, similarly to above in  $K_{i2}$ , that  $\phi(m_j \sigma_{ij}^{-1})$ ,  $\sigma_{ij} > 0$  and  $\phi(s_i (\rho_{ij} \sigma_{ij})^{-1})$  extend smoothly (by (13)) to  $\rho_{ij} = 0$  and  $\sigma_{ij} = 0$ . Therefore the local versions  $\mathcal{M}_{b,i2}$  of  $\overline{\mathcal{M}}_b^\pm$ , defined by

$$r_a = \phi(m_j \sigma_{ij}^{-1}), \quad r_b = \gamma^{-1}(1 - \phi(s_i (\rho_{ij} \sigma_{ij})^{-1})),$$

are 3-dimensional attracting and normally critical manifolds of (35) for  $\mu = 0$  with non-trivial eigenvalues  $-1$  and  $-\gamma < 0$ .

## 2.4 Analysis in the charts $K_{ij}$ used to cover the blow-up of $\overline{\Sigma}_a$

Finally, we consider the equations in charts  $K_{ij}$  with  $(i, j) \in \{4, 5\} \times \{1, 2, 3\}$ , which cover the blow-up of  $\overline{\Sigma}_a$ . The equations in the charts  $K_{i2}$  are given by

$$\begin{aligned} r'_a &= \phi(s_i \rho_{i2}^{-1}) - r_a, \\ r'_b &= 1 - \phi(u_{i2}) - \gamma r_b, \\ u'_{i2} &= \mu G_a(r_a, \eta_i \rho_{i2} u_{i2}), \\ \eta'_i &= \mu s_i \eta_i \rho_{i2} G_b(r_b, s_i \eta_i), \\ \rho'_{i2} &= -\mu s_i \rho_{i2}^2 G_b(r_b, s_i \eta_i), \end{aligned} \tag{37}$$

with  $\eta_i \geq 0$ ,  $\rho_{i2} \geq 0$ . Both of the systems defined by (37) are smooth and slow-fast with respect to  $\mu \rightarrow 0$ . Notice, as above, that  $\phi(s_i \rho_{i2}^{-1})$ ,  $\rho_{i2} > 0$ , extends smoothly to  $\rho_{i2} = 0$  since

$$\lim_{\rho_{i2} \rightarrow 0} \phi(s_i \rho_{i2}^{-1}) = \begin{cases} 0 & \text{if } i = 4, \\ 1 & \text{if } i = 5. \end{cases}$$

Here we have again used (13). Therefore the local versions  $\mathcal{M}_{a,i2}$  of  $\overline{\mathcal{M}}_a$ , defined by

$$r_a = \phi(s_i \rho_{i2}^{-1}), \quad r_b = \gamma^{-1}(1 - \phi(u_{i2})),$$

are 3-dimensional attracting and normally critical manifolds of (37) for  $\mu = 0$  with non-trivial eigenvalues  $-1$  and  $-\gamma < 0$ .

The equations in the phase-directional charts  $K_{i1}$  and  $K_{i3}$  are given by

$$\begin{aligned}
r'_a &= \phi(s_i(\rho_{ij}\sigma_{ij})^{-1}) - r_a, \\
r'_b &= 1 - \phi(m_j\sigma_{ij}^{-1}) - \gamma r_b, \\
\rho'_{ij} &= \mu m_j \rho_{ij} \sigma_{ij} [G_a(r_a, m_j \rho_{ij} \eta_i) - s_i m_j \rho_{ij} G_b(r_b, s_i \eta_i)], \\
\eta'_i &= \mu s_i \eta_i \rho_{ij} \sigma_{ij} G_b(r_b, s_i \eta_i), \\
\sigma'_{ij} &= -\mu m_j \sigma_{ij}^2 G_a(r_a, m_j \rho_{ij} \eta_i).
\end{aligned} \tag{38}$$

with  $\rho_{ij} \geq 0$ ,  $\sigma_{ij} \geq 0$ ,  $(i, j) \in \{4, 5\} \times \{1, 3\}$ , and

$$m_j = \begin{cases} -1 & \text{if } j = 1, \\ 1 & \text{if } j = 3. \end{cases}$$

The equations in (38) define four different systems (there are four distinct couples  $\{i, j\}$ ), each of which are smooth and slow-fast with respect to  $\mu \rightarrow 0$ . Notice again that  $\phi(s_i(\rho_{ij}\sigma_{ij})^{-1})$  and  $\phi(m_j\sigma_{ij}^{-1})$  both extend smoothly (by (13)) to  $\rho_{ij} = 0$  and  $\sigma_{ij} = 0$ . Therefore the local versions  $\mathcal{M}_{a,ij}$  of  $\overline{\mathcal{M}}_a^\pm$  defined by

$$r_a = \phi(s_i(\rho_{ij}\sigma_{ij})^{-1}), \quad r_b = \gamma^{-1}(1 - \phi(m_j\sigma_{ij}^{-1})),$$

are 3-dimensional attracting and normally hyperbolic critical manifolds of (38) for  $\mu = 0$  with non-trivial eigenvalues  $-1$  and  $-\gamma < 0$ .

### 3 Proofs

We are now in a position to prove Theorem 1.2. We prove each assertion of Theorem 1.2 in the following subsections.

#### 3.1 Assertion 1

By working in the 13 different charts (34), which cover  $\overline{\mathbb{P}}$ , we have in shown Section 2 that (7) defines an attracting and normally hyperbolic critical manifold  $\overline{\mathcal{M}} \subset \overline{\mathbb{P}}$ ; in particular, the nontrivial eigenvalues were  $-1$  and  $-\gamma < 0$  in all charts. In this way, by fixing  $k \in \mathbb{N}$  and a compact submanifold  $\overline{\mathcal{M}}_0 \subset \overline{\mathcal{M}}$ , we obtain a  $C^k$ -smooth locally invariant and attracting slow manifold  $\overline{\mathcal{M}}_\mu$  for all  $0 < \mu < \mu_0$  by [11, Thm. 9.1] (for some sufficiently small  $\mu_0 > 0$ ). This slow manifold is  $C^k$   $\mathcal{O}(\mu)$ -close to the unperturbed manifold  $\overline{\mathcal{M}}_0$  on  $\overline{\mathbb{P}}$  (in particular, in the 13 different charts). Next, we notice that the blow-up maps  $\overline{\Phi}$ ,  $\overline{\Phi}_b^\pm$  and  $\overline{\Phi}_a^\pm$  are diffeomorphisms for  $\eta > 0$  and  $\rho > 0$ ; in particular (19), (31) and (33) define (local) diffeomorphisms for  $\eta_i > 0$  and  $\rho_{ij} > 0$ . Consequently, upon applications of these maps, we obtain a ‘blown-down’ version  $\mathcal{M}_\mu$  of  $\overline{\mathcal{M}}_\mu \cap \{\eta > 0, \rho > 0\}$ , which is locally invariant for (12) in the  $(r_a, r_b, p_a, p_b, \sigma)$ -space with  $0 < \sigma < \sigma_0$ . Since  $\sigma' = 0$ , it follows that

$$\mathcal{M}_\mu = \bigcup_{\sigma \in (0, \sigma_0)} \mathcal{M}_\mu(\sigma) \times \{\sigma\},$$

where  $\mathcal{M}_\mu(\sigma)$  is locally invariant for system (4) for all  $0 < \sigma < \sigma_0$ . This completes the proof of assertion 1 in Theorem 1.2.

#### 3.2 Assertion 2

In this section, we work with system (20), which we recall here for convenience in the following form:

$$\begin{aligned}
r'_a &= \phi(v_2) - r_a, \\
r'_b &= 1 - \phi(u_2) - \gamma r_b, \\
u'_2 &= \mu G_a(r_a, \sigma u_2), \\
v'_2 &= \mu G_b(r_b, \sigma v_2),
\end{aligned} \tag{39}$$

where we used the fact that  $\eta_2 = \sigma$ . We consider  $\mu$  and  $\sigma$  as independent small parameters. We are interested in the dynamics on the two-dimensional slow manifold  $\mathcal{M}_{\mu,2} = \mathcal{M}_{\mu,2}(\sigma)$  of (39), see Lemma 2.1. Restricting (20) to  $\mathcal{M}_{\mu,2}(\sigma)$ , we obtain the planar system

$$\begin{aligned}\dot{u}_2 &= G_a(\phi(v_2), \sigma u_2) + \mu \xi_a e^{-\sigma u_2} \Omega_a(u_2, v_2, \sigma) + \mathcal{O}(\mu^2), \\ \dot{v}_2 &= \delta (G_b(\gamma^{-1}(1 - \phi(u_2)), \sigma v_2) + \mu \xi_b e^{-\sigma v_2} \Omega_b(u_2, v_2, \sigma) + \mathcal{O}(\mu^2)),\end{aligned}\quad (40)$$

where the  $\mathcal{O}(\mu^2)$  terms are uniform with respect to  $\sigma$ . In particular, since (39) depends regularly upon  $\sigma$ , these  $C^k$ -smooth remainder terms can in this chart be differentiated with respect to  $u_2, v_2$  and  $\sigma$  without changing the order.

The limiting/reduced flow on  $\mathcal{M}_{2,\mu}(\sigma)$  when  $\mu = \sigma = 0$  is governed by the system

$$\begin{aligned}\dot{u}_2 &= \xi_a \phi(v_2) - 1, \\ \dot{v}_2 &= \delta (\xi_b \gamma^{-1}(1 - \phi(u_2)) - 1),\end{aligned}\quad (41)$$

which has a unique equilibrium point

$$q_2 : (u_2^*, v_2^*) = (\ln(\xi_b - \gamma) - \ln(\gamma), -\ln(\xi_a - 1))$$

if and only if  $\xi_a > 1$  and  $\xi_b > \gamma$ . Using this fact and applying the implicit function theorem, it follows that for each fixed choice of  $\xi_a > 1, \xi_b > \gamma$ , system (20) has a unique equilibrium

$$q_{2,\mu,\sigma} = q_2 + \mathcal{O}(\mu, \sigma), \quad (42)$$

for all  $\mu, \sigma > 0$  sufficiently small. The Jacobian matrix associated with the reduced system (41) is given by

$$J_0(u_2, v_2) = \begin{pmatrix} 0 & \xi_a \phi(v_2)(1 - \phi(v_2)) \\ -\delta \xi_b \gamma^{-1} \phi(u_2)(1 - \phi(u_2)) & 0 \end{pmatrix}.$$

Since  $\text{tr } J_0(u_2, v_2) \equiv 0$  and  $\det J_0(u_2, v_2) > 0$  for all  $(u_2, v_2) \in \mathbb{R}^2$  and  $(\xi_a, \xi_b) \in (1, \infty) \times (\gamma, \infty)$ , it follows that  $q_2$  is a center.

**Remark 3.1.** *Although we do not use the symmetry explicitly, we note that the limiting system in (41) is Hamiltonian with Hamiltonian function*

$$H(u_2, v_2) := \frac{\delta \xi_b}{\gamma} \ln(1 + e^{u_2}) + \xi_a \ln(1 + e^{v_2}) - \delta \left( \frac{\xi_b}{\gamma} - 1 \right) u_2 - v_2.$$

In order to determine the stability of  $q_{2,\mu,\sigma}$ , we need to look to the next order in  $\mu, \sigma$ . Let  $J_{\mu,\sigma}(u_2, v_2)$  denote the Jacobian matrix associated with system (40). Direct calculations together with our calculations for  $\mu = \sigma = 0$  show that

$$\begin{aligned}\text{tr } J_{\mu,\sigma}(u_2, v_2) &= -\sigma [\xi_a \phi(v_2) e^{-\sigma u_2} + \delta \xi_b \gamma^{-1} (1 - \phi(u_2)) e^{-\sigma v_2}] \\ &\quad + \mu \left[ \xi_a \frac{\partial}{\partial u_2} (e^{-\sigma u_2} \Omega_a(u_2, v_2, \sigma)) + \delta \xi_b \frac{\partial}{\partial v_2} (e^{-\sigma v_2} \Omega_b(u_2, v_2, \sigma)) \right] + \mathcal{O}(\mu^2).\end{aligned}$$

Expanding about  $\sigma = 0$ , using that

$$\begin{aligned}\frac{\partial \Omega_a}{\partial u_2} &= \delta \xi_b \gamma^{-1} \phi(u_2)(1 - \phi(u_2)) \phi(v_2) h^-(v_2) + \mathcal{O}(\sigma), \\ \frac{\partial \Omega_b}{\partial v_2} &= \gamma^{-2} \xi_a \phi(u_2)(1 - \phi(u_2)) \phi(v_2)(1 - \phi(v_2)) + \mathcal{O}(\sigma),\end{aligned}$$

which follows from (23), and evaluating the expression at  $q_{\mu,\sigma,2}$ , leads to the asymptotic formula

$$\text{tr } J_{\mu,\sigma}(q_{\mu,\sigma,2}) = -\sigma(1 + \delta) + \mu \frac{(\xi_a - 1)(\xi_b - \gamma)}{\xi_a \xi_b} \frac{\delta(1 + \gamma)}{\gamma} + \mathcal{O}(|(\mu, \sigma)|^2). \quad (43)$$

**Lemma 3.2.** *Suppose  $(\xi_a, \xi_b) \in \Lambda$ , for some compact and connected set  $\Lambda \subset (1, \infty) \times (\gamma, \infty)$ . There exists a  $\sigma_0 > 0$  and a  $C^k$ -smooth function  $\mu_{\text{Hopf}} : \Lambda \times [0, \sigma_0] \rightarrow \mathbb{R}$  such that system (39) undergoes Hopf bifurcations if and only if*

$$\mu = \mu_{\text{Hopf}}(\xi_a, \xi_b, \sigma).$$

Here  $\mu_{\text{Hopf}}(\xi_a, \xi_b, 0) = 0$  and

$$\frac{\partial \mu_{\text{Hopf}}}{\partial \sigma}(\xi_a, \xi_b, 0) = \frac{\xi_a \xi_b}{(\xi_a - 1)(\xi_b - \gamma)} \frac{\gamma(1 + \delta)}{\delta(1 + \gamma)}. \quad (44)$$

*Proof.* Hopf bifurcations are characterized by  $\text{tr } J_{\mu, \sigma}(q_{\mu, \sigma, 2}) = 0$  and  $\det J_{\mu, \sigma}(q_{\mu, \sigma, 2}) > 0$ . Since we have  $\det J_0(q_2) \neq 0$  and

$$\text{tr } J_0(q_2) = 0, \quad \left. \frac{\partial \text{tr } J_{\mu, \sigma}(q_{\mu, \sigma, 2})}{\partial \mu} \right|_{\mu = \sigma = 0} = \frac{(\xi_a - 1)(\xi_b - \gamma)}{\xi_a \xi_b} \frac{\delta(1 + \gamma)}{\gamma} \neq 0,$$

we obtain the function  $\mu_{\text{Hopf}}$  by solving  $\text{tr } J_{\mu, \sigma}(q_{\mu, \sigma, 2}) = 0$  locally for  $\mu$  as a smooth function of  $(\xi_a, \xi_b) \in \Lambda$  and  $0 \leq \sigma < \sigma_0$ , for  $\sigma_0 > 0$  small enough, using the implicit function theorem.  $\square$

**Remark 3.3.** *It is easy to show that the Hopf bifurcation in Lemma 3.2 is unfolded with respect to  $(\xi_a, \xi_b)$ , but we have not been able to analyze the Lyapunov coefficient (see e.g. [3, p. 211]) analytically. The expressions are overwhelming. However, numerical investigations in MatCont [7] suggest that the bifurcation is always supercritical.*

We are now in a position to state and prove a more precise version of Theorem 1.2 assertion 2.

**Proposition 3.4.** *Recall the definition of  $\alpha > 0$  in (11) and consider system (39) along rays in the  $(\sigma, \mu)$ -plane defined by  $\mu = c\sigma$ ,  $\sigma > 0$ , with  $c > 0$ ,  $c \neq \alpha$ , fixed. Then there are only Hopf bifurcations (for  $0 < \sigma \ll 1$ ) along such rays with  $c > \alpha$ . More precisely, we have the following:*

1. *Suppose that  $c > \alpha$ . Then there is a  $\sigma_0 > 0$  small enough such that for all  $0 < \sigma < \sigma_0$  the system (39) with  $\mu = c\sigma$  has a Hopf bifurcation for some  $(\xi_a, \xi_b) \in (1, \infty) \times (\gamma, \infty)$ .*
2. *Suppose that  $0 < c < \alpha$  and fix any compact domain  $\Lambda \subset (1, \infty) \times (\gamma, \infty)$ . Then there is a  $\sigma_0 > 0$  small enough such that for all  $0 < \sigma < \sigma_0$  the system (39) with  $\mu = c\sigma$  and bifurcation parameters  $(\xi_a, \xi_b) \in \Lambda$  does not support a Hopf bifurcation.*

*Proof.* Given that  $\mu = c\sigma$ , we conclude by Lemma 3.2 that we have a Hopf bifurcation if and only if

$$\mu = c\sigma = \mu_{\text{Hopf}}(\xi_a, \xi_b, \sigma) = \frac{\partial \mu_{\text{Hopf}}}{\partial \sigma}(\xi_a, \xi_b, 0)\sigma + \mathcal{O}(\sigma^2),$$

or

$$c = \frac{\partial \mu_{\text{Hopf}}}{\partial \sigma}(\xi_a, \xi_b, 0) + \mathcal{O}(\sigma). \quad (45)$$

The main insight is then that the function

$$(\xi_a, \xi_b) \mapsto \frac{\partial \mu_{\text{Hopf}}}{\partial \sigma}(\xi_a, \xi_b, 0), \quad \xi_a > 1, \xi_b > \gamma,$$

is surjective on the interval  $(\alpha, \infty)$ . This follows directly from (44). Consequently, if  $c > \alpha$  then we can solve (45) for some  $(\xi_a, \xi_b)$  for all  $0 < \sigma \ll 1$  and there is a Hopf bifurcation. In contrast, if  $c < \alpha$  and we fix  $\Lambda$ , then the right hand side of (45) is strictly less than  $\alpha$  for all  $0 < \sigma \ll 1$  and all  $(\xi_a, \xi_b) \in \Lambda$ , in which case there is no Hopf bifurcation.  $\square$

**Remark 3.5.** *In assertion 1 where  $c > \alpha$ , there are Hopf bifurcations along a curve (a hyperbola for any  $0 < \sigma \ll 1$ , see Figure 6 (b) below) in the  $(\xi_a, \xi_b)$ -plane. To see this, notice that for each  $\xi_b > \gamma$  ( $\xi_a > 1$ ), we can solve (45) for  $\xi_a > 1$  ( $\xi_b > \gamma$ , respectively) for all  $0 < \sigma \ll 1$ .*

### 3.3 Assertion 3

In this section, we suppose that  $\mu > 0$  is fixed as  $\sigma \rightarrow 0$ . We then consider system (4) with  $\varepsilon = \mu\sigma$  in the following form:

$$\begin{aligned} r'_a &= \phi(\sigma^{-1} \log p_b) - r_a, \\ r'_b &= 1 - \phi(\sigma^{-1} \log p_a) - \gamma r_b, \\ p'_a &= \mu\sigma(\xi_a r_a - p_a), \\ p'_b &= \mu\sigma\delta(\xi_b r_b - p_b). \end{aligned} \tag{46}$$

Now,  $\mathcal{M}(\sigma)$  is given by

$$r_a = \phi(\sigma^{-1} \log p_b), \quad r_b = \gamma^{-1}(1 - \phi(\sigma^{-1} \log p_a)). \tag{47}$$

We then consider the Lie-derivative  $\mathcal{L}$  of the function

$$(r_a, r_b, p_a, p_b) \mapsto r_a - \phi(\sigma^{-1} \log p_b),$$

in the direction of the vector-field induced by (46) at a point on  $\mathcal{M}(\sigma)$  with  $p_a > 1$  and  $p_b = 1$ . This gives

$$\mathcal{L} = -\phi'(0)\mu\delta(\xi_b\gamma^{-1}(1 - \phi(\sigma^{-1} \log p_a)) - 1) = \frac{1}{4}\mu\delta(1 + \mathcal{O}(\sigma)).$$

Since  $\mathcal{L} > c > 0$  for a positive constant  $c$  for all  $0 < \sigma \ll 1$ , there can be no invariant manifold  $o(1)$ -close to  $\mathcal{M}(\sigma)$  as  $\sigma \rightarrow 0$  in a uniform neighbourhood of this point. The result therefore follows upon letting  $K'$  be so that  $(p_a, 1) \in K'$  for some  $p_a > 1$ . (Of course, we could also have arrived at the same result by working along  $p_a = 1$ .)  $\square$

## 4 Dynamics

In this section, we combine the results in Theorem 1.2 with analytical and numerical investigations into the dynamics of system (4). We start with the following result.

**Lemma 4.1.** *System (4) with  $\sigma, \varepsilon > 0$  has a unique equilibrium  $q : (r_a^*, r_b^*, \xi_a r_a^*, \xi_b r_b^*)$ , where the coordinates  $(r_a^*, r_b^*) \in (0, 1/\xi_a) \times (1/\gamma\xi_b)$  are uniquely determined by the equations*

$$r_a = h^+(\xi_b r_b; 1, \sigma^{-1}), \quad r_b = \gamma^{-1} h^-(\xi_a r_a; 1, \sigma^{-1}). \tag{48}$$

The location of  $q$  depends on  $\xi_a, \xi_b$  and  $\sigma$ , but not on  $\varepsilon$ .

*Proof.* Equilibria of system (4) with  $\varepsilon > 0$  have to satisfy  $p_a = \xi_a r_a$  and  $p_b = \xi_b r_b$ . Substituting these expressions into  $r'_a = 0$  and  $r'_b = 0$  yields the conditions in (48). The existence of a unique equilibrium point  $q : (r_a^*, r_b^*, \xi_a r_a^*, \xi_b r_b^*)$  follows from the monotonicity properties of the Hill functions  $h^\pm$ , see Figure 1. Indeed, define

$$F(r_a) := r_a - h^+(\xi_b \gamma^{-1} h^-(\xi_a r_a; 1, \sigma^{-1}); 1, \sigma^{-1}). \tag{49}$$

It is clear that (48) is equivalent to the equations

$$F(r_a) = 0, \quad r_b = \gamma^{-1} h^-(\xi_a r_a; 1, \sigma^{-1}).$$

Then since

$$F(0) = -h^+(\xi_b \gamma^{-1} \frac{1}{2}; 1, \sigma^{-1}) < 0, \quad \lim_{r_a \rightarrow \infty} F(r_a) = \infty \quad \text{and} \quad (\partial F / \partial r_a)(r_a) > 0,$$

for all  $\sigma > 0$ , the intermediate value theorem implies the existence of a unique solution  $r_a = r_a^* > 0, r_b = r_b^*$ . Finally, the fact that  $(r_a^*, r_b^*) \in (0, 1/\xi_a) \times (0, 1/\gamma\xi_b)$  follows from the expressions in (48) and the fact that range of the Hill functions  $h^\pm$  is  $(0, 1)$ .  $\square$

Consider the  $(p_a, p_b)$ -plane and let  $I, \dots, IV$  denote the four quadrants that are obtained from the partition induced by  $\tilde{\Sigma} = \tilde{\Sigma}_a \cup \tilde{\Sigma}_b$ , where

$$\tilde{\Sigma}_a := \{(1, p_b) : p_b \geq 0\}, \quad \tilde{\Sigma}_b := \{(p_a, 1) : p_a \geq 0\}, \quad (50)$$

see also Figure 5 (a). The fact that QSSR is valid uniformly in  $\sigma$  in regions of the phase space that are bounded away from  $\Sigma$  (recall Remark 1.4), motivates us to consider the QSSR system (6) in the singular limit  $\sigma \rightarrow 0$ . This is a piecewise-linear (PWL) system of the form

$$\begin{aligned} I : \begin{cases} \dot{p}_a &= -p_a, \\ \dot{p}_b &= \delta \left( \frac{\xi_b}{\gamma} - p_b \right), \end{cases} & \quad II : \begin{cases} \dot{p}_a &= -p_a, \\ \dot{p}_b &= -\delta p_b, \end{cases} \\ III : \begin{cases} \dot{p}_a &= \xi_a - p_a, \\ \dot{p}_b &= -\delta p_b, \end{cases} & \quad IV : \begin{cases} \dot{p}_a &= \xi_a - p_a, \\ \dot{p}_b &= \delta \left( \frac{\xi_b}{\gamma} - p_b \right), \end{cases} \end{aligned} \quad (51)$$

where the overdot denotes differentiation with respect to slow time  $\tau = \varepsilon t$  and  $\tilde{\Sigma}$  is the switching manifold. As all four systems in (51) are linear and decoupled, they can easily be solved directly. We omit the calculations here because they will not be necessary for our purposes, however, we summarise a number of important qualitative features of the dynamics in the following result. The proof can be found in Appendix B below.

**Proposition 4.2.** *Consider the PWL protein-only system defined by the systems in (51) on  $\mathbb{R}^2 \setminus \tilde{\Sigma}$ . The following assertions are true:*

- (i) *For all  $(\xi_a, \xi_b) \in \mathbb{R} \cup [0, 1)$  there is a unique equilibrium  $q_{III} : (0, \xi_b/\gamma) \in III$ , which is a stable node.*
- (ii) *For all  $(\xi_a, \xi_b) \in [0, 1) \cup (\gamma, \infty)$  there is a unique equilibrium  $q_{II} : (\xi_a, \xi_b/\gamma) \in II$ , which is a stable node.*
- (iii) *There are no equilibria on  $\mathbb{R}^2 \setminus \tilde{\Sigma}$  when  $(\xi_a, \xi_b) \in (1, \infty) \cup (\gamma, \infty)$ .*
- (iv) *For fixed  $\xi_a \in [0, 1)$ ,*

$$\lim_{\xi_b \rightarrow \gamma^-} q_{III} = (0, 1) \in \tilde{\Sigma}_b.$$

- (v) *For fixed  $\xi_a \in [0, 1)$ ,*

$$\lim_{\xi_b \rightarrow \gamma^+} q_{II} = (\xi_a, 1) \in \tilde{\Sigma}_b.$$

- (vi) *For fixed  $\xi_b \in [0, \gamma)$ ,*

$$\lim_{\xi_a \rightarrow 1^-} q_{II} = (1, \gamma^{-1}\xi_b) \in \tilde{\Sigma}_a.$$

- (vii) *For fixed  $\xi_a > 1$ ,*

$$\lim_{\xi_b \rightarrow \gamma^-} q_{III} = (0, 1) \in \tilde{\Sigma}_b.$$

- (viii) *Suppose that  $\xi_a > 1$  and  $\xi_b > \gamma$  and consider  $(p_a, p_b)(0) \neq (1, 1)$ . Then  $(p_a, p_b)(\tau) \rightarrow (1, 1)$  for  $\tau \rightarrow T_{\max}$ , where  $T_{\max} \in (0, \infty]$  is the maximal time of existence.*

**Remark 4.3.** *The phenomenon in (iv)-(vii), where  $q_{III}$  and  $q_{II}$  collide with the different branches of  $\Sigma$ , is known as boundary-equilibrium bifurcation in PWS systems. We refer to [12, 20, 39] for definitions and classifications of ‘generic’ boundary-equilibria bifurcations in planar Filippov systems, and to [22, 23] for detailed analyses and a classification of ‘generic’ singularly perturbed boundary equilibria which occur*

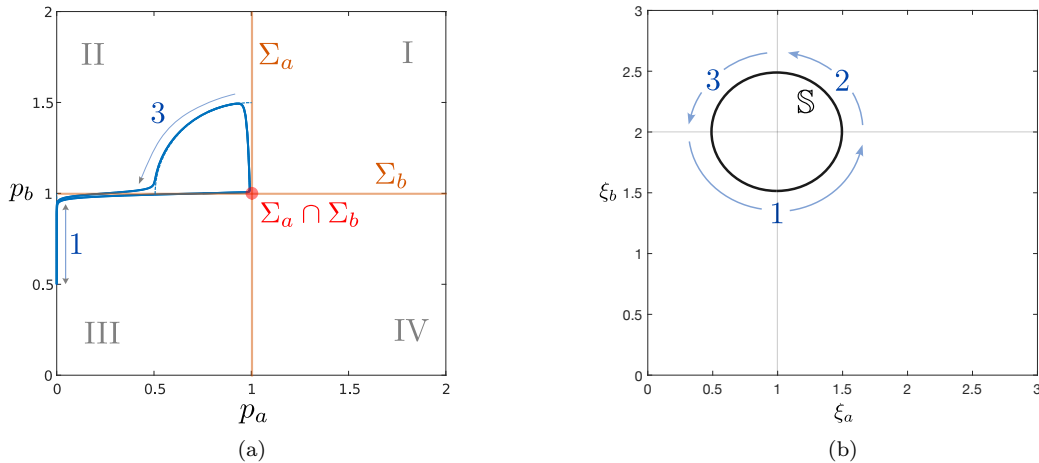


Figure 5: In (a): Projections of the switching manifolds  $\Sigma_a$ ,  $\Sigma_b$  and their intersection  $\Sigma_a \cap \Sigma_b$  in the  $(p_a, p_b)$ -plane are shown in shaded orange and red respectively. A numerical continuation, in which the  $(p_a, p_b)$ -coordinates of the unique equilibrium  $q$  of system (4) for parameter values  $\varepsilon = 5 \times 10^{-5}$ ,  $\sigma = 10^{-2}$ ,  $\gamma = 2$ ,  $\delta = 3$ , and  $(\xi_a, \xi_b)$ -values in a circle  $\mathbb{S}$  of radius  $1/2$  centered at  $(1, \gamma) = (1, 2)$ , is overlaid in blue. The dashed blue line in regions II and III show  $q_{II}$  (barely visible along  $p_a = 0$ ) and  $q_{III}$  from Proposition 4.2. In (b): The circle  $\mathbb{S}$  in  $(\xi_a, \xi_b)$ -space which corresponds to the set of points on the closed blue loop in the left panel figure is shown in black. The labels “1” and “3” correspond to the parts of the loop in the left panel figure with the corresponding label. The label “2” does not appear in (a) because it is ‘hidden’ near  $\Sigma_a \cap \Sigma_b$  (it is described in the scaled coordinates of  $K_2$ ).

in smooth planar systems that limit to a PWS system (as is the case for system (4) when  $\sigma \rightarrow 0$ ). We also refer to [33], where a singularly perturbed boundary-node bifurcation is shown to play an important role in describing the rapid onset of large amplitude oscillations in a model for substrate-depletion oscillation. The cases in (iv)-(vii) in Proposition 4.2 are examples of degenerate boundary-node bifurcations. The degeneracy stems from the fact that  $q_{III}$  and  $q_{II}$  have an associated eigenvector which intersects  $\tilde{\Sigma}$  non-transversally at the collision.

Now consider a circle  $\mathbb{S}$  in the  $(\xi_a, \xi_b)$  parameter plane of radius  $< \min\{1, \gamma\}$  centered around  $(1, \gamma)$ , see Figure 5 (b). We consider  $\gamma = 2$ ,  $\delta = 3$  and a radius equal to  $\frac{1}{2}$  to be specific. Then on the lower left part of  $\mathbb{S}$ , where  $\xi_a < 1$  and  $\xi_b < \gamma = 2$ ,  $q_{III}$  of Proposition 4.2 traces out a curve in the  $(p_a, p_b)$ -plane which is shown in dashed blue in Figure 5 (a) (it is contained within  $p_a = 0$  and is barely visible because it aligns with the blue curve). Similarly on the upper left part of  $\mathbb{S}$ , where  $\xi_a < 1$  and  $\xi_b > \gamma = 2$ ,  $q_{II}$  of Proposition 4.2 traces out a curve (also a quarter circle and shown in dashed blue in Figure 5 (a)). We then perform numerical computations for  $\varepsilon = 5 \times 10^{-5}$ ,  $\sigma = 10^{-2}$  (and therefore  $\mu = 5 \times 10^{-3}$  cf. (10)), to follow the unique equilibrium  $q$  of system (4) as  $(\xi_a, \xi_b)$  transverses around  $\mathbb{S}$ . We describe the results as below.

We start with a  $(\xi_a, \xi_b)$  value within the lower left quadrant of  $\mathbb{S}$ , in which case assertion (i) of Proposition 4.2 implies the existence of a stable node  $q_{III}$ . As we begin to move counterclockwise around  $\mathbb{S}$ ,  $q$  initially moves down the vertical axis until it reaches a minimum for parameter values at the ‘south pole’ of  $\mathbb{S}$ , after which it begins to move up the  $p_b$ -axis. This accounts for part ‘1’ of the loop depicted in Figure 5 (b) and is in agreement with the corresponding path of  $q_{III}$  (in dashed blue) of Proposition 4.2. The degenerate boundary-node bifurcation described in assertion (iv) of Proposition 4.2 occurs as  $\xi_b/\gamma$  approaches 1 from below and  $q$  collides with  $\tilde{\Sigma}_b$ , i.e. as we approach the right-most point of  $\mathbb{S}$  from below. Due to assertion (iii) of Proposition 4.2, there are no equilibria of system (51) on  $\mathbb{R}^2 \setminus \tilde{\Sigma}$  as we continue along the top right quadrant of  $\mathbb{S}$ ; this is part ‘2’ of the loop. As we continue into the top left quadrant of  $\mathbb{S}$ , the equilibrium  $q \in IV$  ‘emerges’ from  $\tilde{\Sigma}_a$  via the degenerate boundary-node bifurcation described in assertion (vi) of Proposition 4.2. The equilibrium  $q$  subsequently follows a path determined by  $q_{II}$  (in dashed blue) until it collides with  $\tilde{\Sigma}_b$  from above as the left-most point of  $\mathbb{S}$

is approached from above (corresponding to the degenerate boundary-node described in assertion (v)); this is part ‘3’ of the loop. Finally, in accordance with assertion (vii),  $q$  emerges from  $\tilde{\Sigma}_b$  via another degenerate boundary-node bifurcation, and moves into  $III$  as we move back into the lower left quadrant of  $\mathbb{S}$ , thereby completing the loop. Numerically we find that the equilibrium remains stable throughout (and the global attractor).

These results are consistent with Theorem 1.2. In fact, Fenichel’s theory guarantees that the qualitative dynamics of the original 4-dimensional model (4) for all  $0 < \varepsilon \ll 1$ ,  $0 < \sigma \ll 1$ , are captured by (51) and Proposition 4.2 as long as we stay uniformly away from  $\Sigma$ ; notice, cf. Remark 1.4, that this does not rely on (10). However, when  $\xi_a > 1$  and  $\xi_b > \gamma$ , assertion (iii) in Proposition 4.2 states that the limiting PWL system (51) does not have an equilibrium on  $\mathbb{R}_+^2 \setminus \tilde{\Sigma}$ . To track  $q$  within this parameter regime we can work on the local version of  $\mathcal{M}_\mu(\sigma)$  in the chart  $K_2$ , recall (19), Section 3.2 and (42) specifically. The coordinates in  $K_2$  provide a zoom near  $\Sigma_a \cap \Sigma_b$ ; this is consistent with Figure 5 (part ‘2’ of  $\mathbb{S}$ ) where  $q$  remains close to  $\Sigma_a \cap \Sigma_b$ . We also expect that it is possible to track  $q$  on the remaining parts of  $\mathbb{S}$ , near  $\xi_a \approx 1$  and  $\xi_b \approx \gamma$ , by working on the local versions of  $\mathcal{M}_\mu(\sigma)$  in the charts  $K_{ij}$ ,  $i \in \{1, 3, 4, 5\}$ . This will involve further parameter blow-up, see e.g. [1, 23, 33].

In Figure 6, we repeat the numerical computations with the same data that was used to generate Figure 5 except that  $\varepsilon$  has increased from  $5 \times 10^{-5}$  to  $5 \times 10^{-3}$  (so that  $\mu = \frac{1}{2}$  in Figure 6, cf. (10)). Following this increase in  $\varepsilon$ , we now identify two supercritical Hopf bifurcations using MatCont [7] as we traverse the same circle in the  $(\xi_a, \xi_b)$ -plane. Figure 6 (b) shows the output of a 2-parameter continuation in MatCont [7] of the Hopf curve (note that the two bifurcations points in Figure 6 (a) correspond to two distinct points on this curve). Stable limit cycles are observed numerically in the region bounded above this curve.

The Hopf bifurcations are in agreement with Theorem 1.2, see also Section 3.2 and Lemma 3.2 specifically. In fact, with  $\gamma = 2$  and  $\delta = 3$  we obtain that

$$\alpha = \frac{8}{9},$$

recall (11). Therefore with the values in Figure 5, we have

$$\mu = 5 \times 10^{-3} < \alpha\sigma = \frac{8}{9} \times 10^{-2},$$

and the absence of a Hopf bifurcation is therefore consistent with assertion 2 of Theorem 1.2. In contrast, with the values in Figure 5, we have

$$\mu = \frac{1}{2} > \alpha\sigma = \frac{8}{9} \times 10^{-2},$$

and the existence of a Hopf bifurcation is therefore consistent with assertion 2 of Theorem 1.2. Moreover, the observed existence of stable limit cycles in the region bounded above the curve in Figure 6 (b) is consistent with assertion (viii) of Proposition 4.2 and Theorem 1.2. Indeed, by assertion 1 of Theorem 1.2 we can reduce the system to a 2-dimensional locally invariant manifold  $\mathcal{M}_\mu(\sigma)$  and for the values in the region bounded above the curve in Figure 6 (b) the equilibrium is an unstable focus, see Section 3.2. We can therefore obtain existence of a limit cycle using the Poincaré-Bendixson theorem. In fact, assertion (viii) of Proposition 4.2 shows that the limit cycles are  $o(1)$ -close to  $(p_a, p_b) = (1, 1)$  in the  $(p_a, p_b)$ -plane with respect to  $\mu, \sigma \rightarrow 0$ .

## 5 Discussion and outlook

The analysis and results in this article show, in the context of the activator-inhibitor model (4), that the asymptotic behaviour of GRN models in general form (1) as  $(\varepsilon, \sigma) \rightarrow (0, 0)$  may depend in an important way on *how* this limit is taken. Theorem 1.2 assertion 1 asserts the existence of a ‘global’ 2-dimensional, attracting invariant manifold  $\mathcal{M}_\mu(\sigma)$ , upon which the dynamics are governed by a reduced protein-only system, whenever  $0 < \mu = \varepsilon/\sigma \ll 1$ , i.e. when  $0 < \varepsilon \ll \sigma \ll 1$  and  $0 < \sigma < \sigma_0$ ; assertion 3 implies that  $0 < \mu \ll 1$  is also necessary for a global reduction. At the same time, assertion 2 of Theorem 1.2 shows that even when  $0 < \mu = \varepsilon/\sigma \ll 1$  holds true, the dynamics on  $\mathcal{M}_\mu(\sigma)$  still depends on the relative size of  $\mu$  and  $\sigma$ . In particular, Hopf bifurcations only occur when  $\mu > \alpha\sigma$ , see Figure 3 and Proposition 3.4

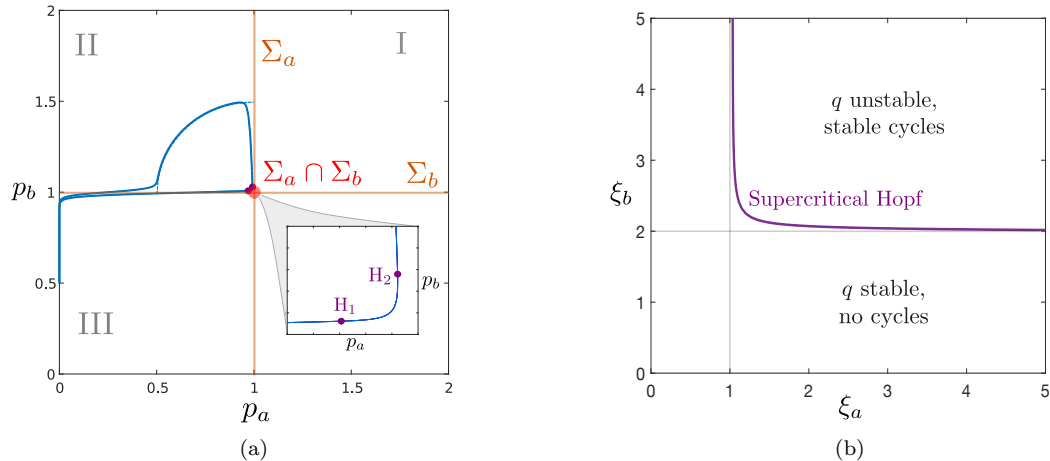


Figure 6: In (a): The diagram obtained by performing the same numerical computations as in Figure 5, except with  $\varepsilon = 5 \times 10^{-3}$  instead of  $5 \times 10^{-5}$  (so that  $\mu = \frac{1}{2}$ ). This time we find two supercritical Hopf bifurcations using MatCont [7] close to the (projection of the) intersection  $\Sigma_a \cap \Sigma_b$ ; these are labelled  $H_1$  and  $H_2$  and indicated by purple discs in the zoom/inset. The first Lyapunov coefficients associated with the Hopf bifurcations  $H_1$  and  $H_2$  were calculated numerically in MatCont to be  $l_1 \approx -0.07676$  and  $l_1 \approx -0.2384$  respectively, indicating that both bifurcations are supercritical. In (b): The Hopf curve in  $(\xi_a, \xi_b)$ -space, shown in purple, appears to asymptote along  $\xi_a = 1$  and  $\xi_b = \gamma = 2$ . The Hopf bifurcations  $H_1$  and  $H_2$  correspond to intersections of this curve with the circle  $\mathbb{S}$  shown in Figure 5 (right).

for a precise statement; in this parameter region we therefore conclude that the QSSR system (6), which does not support Hopf bifurcations or limit cycles, recall Lemma 1.1, is not a faithful representation. The basic reason for this ‘disagreement’, is that the higher order contributions in system (4) on  $\mathcal{M}_\mu(\sigma)$ , which are omitted in system (6), play an important role in determining the qualitative dynamics, see also Remark 3.1.

It seems natural to ask about the extent to which the geometric analysis for the ‘representative’, low-dimensional model (4) presented herein, can be extended to the study of the  $2N$ -dimensional GRN models defined by (1) more generally. Given that the particular form of the equations did not play an important role in the proof of assertion 1 in Theorem 1.2 in particular, it seems natural to ask whether a counterpart can be proven for the  $2N$ -dimensional network (1). These and other related problems are part of on-going work.

## Acknowledgements

SJ was partially supported by European Union Marie Skłodowska-Curie Postdoctoral Fellowship grant 101103827. SJ would also like to thank KUK and the Department of Applied Mathematics and Computer Science for their hospitality during his secondment at the Technical University of Denmark, during which time much of the work presented herein was done.

## References

- [1] L. BAUMGARTNER AND P. SZMOLYAN, *A multiparameter singular perturbation analysis of the Robertson model*, Studies in Applied Mathematics, 154 (2025), p. e70020.
- [2] R. CASEY, H. D. JONG, AND J.-L. GOUZÉ, *Piecewise-linear models of genetic regulatory networks: Equilibria and their stability*, Journal of Mathematical Biology, 52 (2006), pp. 27–56.

- [3] S.-N. CHOW, C. LI, AND D. WANG, *Normal forms and bifurcation of planar vector fields*, Cambridge University Press, , 1994.
- [4] L. P. DA CRUZ AND J. TORREGROSA, *A Bendixon–Dulac theorem for some piecewise systems*, *Nonlinearity*, 33 (2020), p. 2455.
- [5] P. DE MAESSCHALCK AND F. DUMORTIER, *Slow–fast Bogdanov–Takens bifurcations*, *Journal of Differential Equations*, 250 (2011), pp. 1000–1025.
- [6] D. DEL VECCHIO, *Design and analysis of an activator-repressor clock in E. Coli*, in *Proceedings of American Control Conference*, New York, July 2007, IEEE, pp. 1589–1594.
- [7] A. DHOOGHE, W. GOVAERTS, AND Y. A. KUZNETSOV, *MATCONT: a MATLAB package for numerical bifurcation analysis of ODEs*, *ACM Transactions on Mathematical Software (TOMS)*, 29 (2003), pp. 141–164.
- [8] F. DUMORTIER AND R. ROUSSARIE, *Canard cycles and center manifolds*, no. 577 in *Memoirs of the American Mathematical Society*, American Mathematical Society, , 1996.
- [9] L. EDELSTEIN-KESHET, *Mathematical models in biology*, *SIAM Review*, 30 (2005), pp. 296–299.
- [10] R. EDWARDS, A. MACHINA, G. MCGREGOR, AND P. VAN DEN DRIESSCHE, *A modelling framework for gene regulatory networks including transcription and translation*, *Bulletin of Mathematical Biology*, 77 (2015), pp. 953–983.
- [11] N. FENICHEL, *Geometric singular perturbation theory for ordinary differential equations*, *Journal of Differential Equations*, 31 (1979), pp. 53–98.
- [12] A. F. FILIPPOV, *Differential equations with discontinuous right-hand side*, *Matematicheskii sbornik*, 93 (1960), pp. 99–128.
- [13] S. FRIEDER AND P. SZMOLYAN, *Desingularization of discontinuities via blow-up in an ODE-model of a gene regulatory network*, Master’s thesis, Vienna University of Technology, 2018.
- [14] M. GAMEIRO, T. GEDEON, H. KOKUBU, K. MISCHAIKOW, H. OKA, B. RIVAS, E. VIEIRA, AND D. GAMEIRO, *Global dynamics of ordinary differential equations: Wall labelings, Conley complexes, and ramp systems*, arXiv preprint arXiv:2412.11078, (2024).
- [15] J. GARCIA-OJALVO, M. B. ELOWITZ, AND S. H. STROGATZ, *Modeling a synthetic multicellular clock: Repressilators coupled by quorum sensing*, *Proceedings of the National Academy of Sciences*, 101 (2004), pp. 10955–10960.
- [16] T. GEDEON, G. CUMMINS, AND J. J. HEYS, *Effect of model selection on prediction of periodic behavior in gene regulatory networks*, *Bulletin of Mathematical Biology*, 74 (2012), pp. 1706–1726.
- [17] L. GLASS AND S. A. KAUFFMAN, *The logical analysis of continuous, non-linear biochemical control networks*, *Journal of Theoretical Biology*, 39 (1973), pp. 103–129.
- [18] J.-L. GOUZÉ AND T. SARI, *A class of piecewise linear differential equations arising in biological models*, *Dynamical Systems*, 17 (2002), pp. 299–316.
- [19] R. GUANTES AND J. F. POYATOS, *Dynamical principles of two-component genetic oscillators*, *PLoS Computational Biology*, 2 (2006), p. e30.
- [20] S. J. HOGAN, M. E. HOMER, M. R. JEFFREY, AND R. SZALAI, *Piecewise smooth dynamical systems theory: The case of the missing boundary equilibrium bifurcations*, *Journal of Nonlinear Science*, 26 (2016), pp. 1161–1173.
- [21] L. IRONI, L. PANZERI, E. PLAhte, AND V. SIMONCINI, *Dynamics of actively regulated gene networks*, *Physica D: Nonlinear Phenomena*, 240 (2011), pp. 779–794.
- [22] S. JELBART, K. U. KRISTIANSEN, AND M. WECHSELBERGER, *Singularly perturbed boundary-equilibrium bifurcations*, *Nonlinearity*, 34 (2021), p. 7371.

- [23] ———, *Singularly perturbed boundary-focus bifurcations*, *Journal of Differential Equations*, 296 (2021), pp. 412–492.
- [24] S. JELBART, N. PAGES, V. KIRK, J. SNEYD, AND M. WECHSELBERGER, *Process-oriented geometric singular perturbation theory and calcium dynamics*, *SIAM Journal on Applied Dynamical Systems*, 21 (2022), pp. 982–1029.
- [25] C. K. JONES, *Geometric singular perturbation theory*, in *Dynamical systems (Montecatini Terme, 1994)*, vol. 1609 of *Lecture Notes in Mathematics*, Springer, Berlin, 1995, pp. 44–118.
- [26] P. KAKLAMANOS AND K. U. KRISTIANSEN, *Regularization and geometry of piecewise smooth systems with intersecting discontinuity sets*, *SIAM Journal on Applied Dynamical Systems*, 18 (2019), pp. 1225–1264.
- [27] I. KOSIUK AND P. SZMOLYAN, *Geometric analysis of the Goldbeter minimal model for the embryonic cell cycle*, *Journal of Mathematical Biology*, 72 (2016), pp. 1337–1368.
- [28] K. U. KRISTIANSEN, *The regularized visible fold revisited*, *Journal of Nonlinear Science*, 30 (2020), pp. 2463–2511.
- [29] ———, *Blowup analysis of a hysteresis model based upon singular perturbations*, *Journal of Nonlinear Science*, 34 (2024), p. 6.
- [30] K. U. KRISTIANSEN AND S. J. HOGAN, *On the use of blowup to study regularizations of singularities of piecewise smooth dynamical systems in  $\mathbb{R}^3$* , *SIAM Journal on Applied Dynamical Systems*, 14 (2015), pp. 382–422.
- [31] ———, *Regularizations of two-fold bifurcations in planar piecewise smooth systems using blowup*, *SIAM Journal on Applied Dynamical Systems*, 14 (2015), pp. 1731–1786.
- [32] ———, *Resolution of the piecewise smooth visible–invisible two-fold singularity in  $\mathbb{R}^3$  using regularization and blowup*, *Journal of Nonlinear Science*, 29 (2019), pp. 723–787.
- [33] K. U. KRISTIANSEN AND P. SZMOLYAN, *Relaxation oscillations in substrate-depletion oscillators close to the nonsmooth limit*, *Nonlinearity*, 34 (2021), p. 1030.
- [34] N. KRUFF, C. LÜDERS, O. RADULESCU, T. STURM, AND S. WALCHER, *Algorithmic reduction of biological networks with multiple time scales*, *Mathematics in Computer Science*, 15 (2021), pp. 499–534.
- [35] M. KRUPA AND P. SZMOLYAN, *Extending geometric singular perturbation theory to nonhyperbolic points—fold and canard points in two dimensions*, *SIAM Journal on Mathematical Analysis*, 33 (2001), pp. 286–314.
- [36] ———, *Relaxation oscillation and canard explosion*, *Journal of Differential Equations*, 174 (2001), pp. 312–368.
- [37] C. KUEHN, *Multiple time scale dynamics*, vol. 191 of *Applied Mathematical Sciences*, Springer, Berlin, 2015.
- [38] C. KUEHN, N. BERGLUND, C. BICK, M. ENGEL, T. HURTH, A. IUORIO, AND C. SORESINA, *A general view on double limits in differential equations*, *Physica D: Nonlinear Phenomena*, 431 (2022), p. 133105.
- [39] Y. A. KUZNETSOV, S. RINALDI, AND A. GRAGNANI, *One-parameter bifurcations in planar Filippov systems*, *International Journal of Bifurcation and Chaos*, 13 (2003), pp. 2157–2188.
- [40] J. LLIBRE, P. R. DA SILVA, AND M. A. TEIXEIRA, *Study of singularities in nonsmooth dynamical systems via singular perturbation*, *SIAM Journal on Applied Dynamical Systems*, 8 (2009), pp. 508–526.
- [41] A. MACHINA, R. EDWARDS, AND P. VAN DEN DRIESSCHE, *Sensitive dependence on initial conditions in gene networks*, *Chaos: An Interdisciplinary Journal of Nonlinear Science*, 23 (2013).

- [42] A. MACHINA, R. EDWARDS, AND P. VAN DEN DRIESSCHE, *Singular dynamics in gene network models*, SIAM Journal on Applied Dynamical Systems, 12 (2013), pp. 95–125.
- [43] A. MACHINA AND A. PONOSOV, *Filippov solutions in the analysis of piecewise linear models describing gene regulatory networks*, Nonlinear Analysis: Theory, Methods & Applications, 74 (2011), pp. 882–900.
- [44] Z. MIAO, N. POPOVIĆ, AND P. SZMOLYAN, *Oscillations in a cAMP signalling model for cell aggregation—a geometric analysis*, Journal of Mathematical Analysis and Applications, 483 (2020), p. 123577.
- [45] E. PLAhte AND S. KJØGLUM, *Analysis and generic properties of gene regulatory networks with graded response functions*, Physica D: Nonlinear Phenomena, 201 (2005), pp. 150–176.
- [46] A. POLYNIKIS, S. HOGAN, AND M. DI BERNARDO, *Comparing different ODE modelling approaches for gene regulatory networks*, Journal of Theoretical Biology, 261 (2009), pp. 511–530.
- [47] G. QUEE AND R. EDWARDS, *Ramp approximations of sigmoid control functions in gene networks*, Physica D: Nonlinear Phenomena, 418 (2021), p. 132840.
- [48] B. RAHMANI, S. JELBART, V. KIRK, AND J. SNEYD, *Understanding broad-spike oscillations in a model of intracellular calcium dynamics*, SIAM Journal on Applied Dynamical Systems, 24 (2025), pp. 131–164.
- [49] J. SIEBER, H. MAHDI, AND K. TSANEVA, *Alpha-delta transitions in cortical rhythms as grazing bifurcations*, The ANZIAM Journal, (2025).
- [50] P. SZMOLYAN AND M. WECHSELBERGER, *Canards in  $\mathbb{R}^3$* , Journal of Differential Equations, 177 (2001), pp. 419–453.
- [51] R. THOMAS, *Boolean formalization of genetic control circuits*, Journal of Theoretical Biology, 42 (1973), pp. 563–585.
- [52] M. WECHSELBERGER, *Geometric singular perturbation theory beyond the standard form*, in Frontiers in Applied Dynamical Systems: Reviews and Tutorials, vol. 6, Springer International Publishing, New York, 2020.
- [53] S. WIDDER, J. SCHICHO, AND P. SCHUSTER, *Dynamic patterns of gene regulation I: Simple two-gene systems*, Journal of Theoretical Biology, 246 (2007), pp. 395–419.
- [54] S. WIGGINS, *Normally hyperbolic invariant manifolds in dynamical systems*, vol. 105, Springer Science & Business Media, New York, 1994.

## A Derivation of the model (4)

The 4-dimensional activator-inhibitor model considered in [46, 53] can be written as

$$\begin{aligned} r'_a &= m_a h^+(p_b; \theta_b, n_b) - \gamma_a r_a, \\ r'_b &= m_b h^-(p_a; \theta_a, n_a) - \gamma_b r_b, \\ p'_a &= \varepsilon (k_a r_a - \delta_a p_a), \\ p'_b &= \varepsilon (k_b r_b - \delta_b p_b), \end{aligned} \tag{52}$$

where, as in the general network (1),  $r_i \geq 0$  represents the concentration of transcribed mRNA associated with a particular gene  $i$ ,  $p_i \geq 0$  represents the concentration of the corresponding translated protein,  $\varepsilon, n_i, m_i, \theta_i, \gamma_i, k_i, \delta_i > 0$  are parameters ( $i \in \{a, b\}$ ) and the dash denotes differentiation with respect to time  $t$ .

The notation and formulation in system (52) agrees with [46, eqn. (41)], except for the following two differences:

- (i) The parameter  $\varepsilon$  in system (52) is actually  $\varepsilon^{-1}$  in [46]. We prefer to work with a small (as opposed to large) parameter  $\varepsilon$ ;
- (ii) System (52) is written on the fast time-scale  $t$ , whereas [46, eqn. (41)] is written on the slow time-scale  $\tau = \varepsilon t$ .

In this paper, we assume that  $n_a = n_b$  and define

$$0 < \sigma := n_a^{-1} = n_b^{-1}. \tag{53}$$

**Lemma A.1.** *Given assumption (53), system (52) is equivalent (by rescalings only) to the system*

$$\begin{aligned} \tilde{r}'_a &= h^+(\tilde{p}_b; 1, \sigma^{-1}) - \tilde{r}_a, \\ \tilde{r}'_b &= h^-(\tilde{p}_a; 1, \sigma^{-1}) - \gamma \tilde{r}_b, \\ \tilde{p}'_a &= \tilde{\varepsilon} (\xi_a \tilde{r}_a - \tilde{p}_a), \\ \tilde{p}'_b &= \tilde{\varepsilon} \delta (\xi_b \tilde{r}_b - \tilde{p}_b), \end{aligned} \tag{54}$$

where the dash now denotes differentiation with respect to  $\tilde{t} = \gamma_a t$ , and

$$\gamma = \frac{\gamma_b}{\gamma_a}, \quad \xi_a = \frac{k_a m_a}{\gamma_a \theta_a}, \quad \xi_b = \frac{k_b m_b}{\gamma_a \theta_b}, \quad \delta = \frac{\delta_b}{\delta_a}, \quad \tilde{\varepsilon} = \frac{\delta_a}{\gamma_a} \varepsilon. \tag{55}$$

*Proof.* Applying the time rescaling  $t = \gamma_a^{-1} \tilde{t}$  and the coordinate rescaling

$$r_a = \frac{m_a}{\gamma_a} \tilde{r}_a, \quad r_b = \frac{m_b}{\gamma_a} \tilde{r}_b, \quad p_a = \theta_a \tilde{p}_a, \quad p_b = \theta_b \tilde{p}_b,$$

yields the desired result.  $\square$

Upon dropping the tildes in (54) we obtain system (4).

## B Proof of Proposition 4.2

Assertions (i)-(vii) follow from direct calculations using the equations in (51) and the definition of the (reduced) switching manifold  $\tilde{\Sigma}$  in (50); the details are omitted for brevity.

We therefore focus on (viii). Consider first an initial condition  $(p_a(0), p_b(0)) = (1, p_b(0))$  with  $p_b(0) > 1$ . It is then elementary (using the piecewise-linear structure of (51)) to show that there are minimal ‘hitting times’  $0 < T_1 < T_2 < T_3 < T_4$  such that  $p_b(T_1) = p_a(T_2) = p_b(T_3) = p_a(T_4) = 1$  and  $p_a(T_1) > 1$ ,  $p_b(T_2) < 1$ ,  $p_a(T_3) < 1$ ,  $p_b(T_4) > 1$ , see also (57) below. This shows that there is a well-defined Poincaré map on  $\{p_a = 1, p_b > 1\}$  given by  $P : p_b(0) \mapsto p_b(T_4)$  with  $p_b(0), p_b(T_4) > 1$ . There can be no fixed-points of this diffeomorphism since the piecewise-linear vector field associated with system (51) has

constant divergence equal to  $-(\delta + 1) < 0$ . This follows from Dulac's theorem which is also applicable in the present context because there is no sliding along the discontinuity sets, only crossing; see e.g. [4].

To complete the proof, we show that  $P$  extends  $C^\infty$ -smoothly to  $p_b = 1$  with

$$P(1) = 1, \quad P'(1) = 1 \quad \text{and} \quad P''(1) = -\frac{(\delta + 1)\xi_a\xi_b}{2\delta(\xi_b - \gamma)} < 0. \quad (56)$$

Indeed, since  $P$  has no fixed-points, it follows that  $1 < P(p_b) < p_b$  for all  $p_b > 1$  and therefore  $P^n(p_b) \rightarrow 1^+$  for  $n \rightarrow \infty$ . To prove (56), we simply solve the linear equations to obtain

$$\begin{cases} p_a(T_1) = \xi_a + (1 - \xi_a)p_b(0)^{-\delta^{-1}}, \\ p_b(T_2) = p_a(T_1)^{-\delta}, \\ p_a(T_3) = \left(\frac{\xi_b - \gamma}{\xi_b - \gamma p_b(T_2)}\right)^{\delta^{-1}}, \\ p_b(T_4) = \xi_b\gamma^{-1} + (1 - \xi_b\gamma^{-1})\left(\frac{\xi_a - 1}{\xi_a - p_a(T_3)}\right)^{\delta}. \end{cases} \quad (57)$$

From these expressions, one may directly realize that  $P$  has a smooth extension to  $p_b(0) = 1$  with  $P(1) = 1$  and  $P'(1) = 1$ . A simple calculation also shows the expression for  $P''(1)$ .